JOURNAL OF GEOPHYSICAL RESEARCH, VOL. 93, NO. B12, PAGES 15,163-15,182, DECEMBER 10, 1988

ACTIVE TECTONICS OF THE EASTERN SUNDA AND BANDA ARCS

Robert McCaffrey[1]

Air Force Geophysics Laboratory, Hanscom Air Force Base, Bedford, Massachusetts

Abstract. The tectonics of the eastern Sunda and Banda arcs of eastern Indonesia are inferred from the centroid depths, seismic moments, and fault plane solutions of 63 large earthquakes that occurred between 1962 and 1984. Source parameters are estimated by inverting long-period, teleseismic P and SH waves. Earthquakes show that the collision of the Australian continent with the Banda arc shortens the upper plate beneath the forearc and back arc basin over the broad area between the Timor and Seram troughs. Along the eastern end of the Sunda arc and along the southern Banda arc, earthquakes reveal that the arc and forearc respond to collision by shortening in the direction of convergence, by elongating in the direction perpendicular to convergence, and by thrusting over the back arc basin. Shallow thrust and strike-slip earthquakes beneath the Banda Basin (the back arc basin) demonstrate that deformation within the back arc accommodates some of the northward motion of the Australian continent. The rate of north-south shortening of the entire upper plate at the longitude of Timor calculated from the seismic moments of the earthquakes over the 22-year period is roughly 20% of the predicted convergence rate between Australia and southeast Asia. Strike-slip faulting within the Banda Basin results also in eastward motion of the Banda arc with respect to western Indonesia and Australia. Eastward extrusion of the Banda arc results in thrusting at the Aru trough. Earthquakes due to thrusting of the back arc basin beneath the volcanic arc are too shallow to corroborate that the arc's polarity has reversed although the Wetar back arc thrust zone at present has a high seismic slip rate. Earthquakes and their mechanisms provide evidence that the lithosphere of the Weber Basin, a 7500-m-deep forearc basin, rests on the subducting lithosphere, without intervening asthenosphere, so that the Weber Basin subsides in response to sinking of the subducting lithosphere. Closure of the Banda Basin is geometrically incompatible with the Australian plate subducting simultaneously beneath both the Timor and Seram troughs. Instead, the Bird's Head, which subducts beneath Seram, is decoupled from the Australian plate in western New Guinea and probably moves west or southwest with respect to Australia. In the eastern Indonesian example, strike-slip faulting plays a major role in the evolution of the collision zone and clearly demonstrates the complexity in three dimensions of continental accretion and mountain building by arc-continent collision.

[1]Now at Department of Geology, Rensselaer Polytechnic Institute, Troy, New York.

Paper number 88JB03315.
0148-0227/88/88JB-03315$05.00

Introduction

Continental lithosphere entering a subduction zone is unlikely to continue the steady state subduction that is characteristic of oceanic lithosphere. If the thickness and low density of its crust prevent it from being subducted to great depths [McKenzie, 1969; Molnar and Gray, 1979], then collision will result and some rearrangement of the plate geometry must occur. Most ideas for the absorption of the postcollision convergence call for redistribution of thrust faulting in two dimensions, such as by forming a new subduction zone elsewhere (possibly of opposite polarity) or by development of a wide zone of underthrusting [McKenzie, 1969]. The continent-continent collision of India with Eurasia, however, demonstrates that the convergence may be taken up by various types of faults distributed over a very wide area [e.g., Molnar and Tapponnier, 1975].

Nevertheless, because oceanic plates typically deform along more discrete zones than do continental plates, we continue to view island arc-continent collisions as resulting in a jump in the locus of subduction rather than in a broad zone of deformation. A widely cited example of this is New Guinea where Australia collided with an island arc in the late Miocene [Dow and Sukamto, 1984]; most interpretations call for a reversal of the arc's polarity [e.g., Cooper and Taylor, 1987; Dewey and Bird, 1970; Hamilton, 1979], but the evidence for it is not unequivocal [Johnson and Jaques, 1980], and the identification of major strike-slip faulting offers alternative possibilities [e.g., Abers and McCaffrey, 1988; Dow and Sukamto, 1984].

Along the eastern Sunda and Banda arcs of eastern Indonesia, the Australian continent is colliding with the Banda island arc (Figure 1), providing the opportunity to study the process of arc-continent collision in action. This section of the Sunda and Banda convergent margin includes the transition from subduction of oceanic lithosphere of the Indian Ocean at the Java trench (west of 120°E) to subduction of the Scott Plateau, probably thinned continental crust [Stagg and Exon, 1981] (120°-123°E), to collision of the thick crust of the Australian continent with the Banda arc (east of 123°E and around the bend into the Seram trough). The frequent large earthquakes can be used to constrain the shallow tectonics of the collision zone, but to separate the shallow earthquakes from those in subducting lithosphere requires greater accuracy in depths than is possible with P wave arrival times or pP-P differential times (the latter because of the difficulty to identify the pP phase correctly). In order to constrain the depths of the earthquakes well enough to be able to interpret their distribution with depth, I invert teleseismic, long-period P and SH waves.

Data and Methods

Approximately 200 earthquakes with body wave magnitudes greater than 5.5 were examined, of

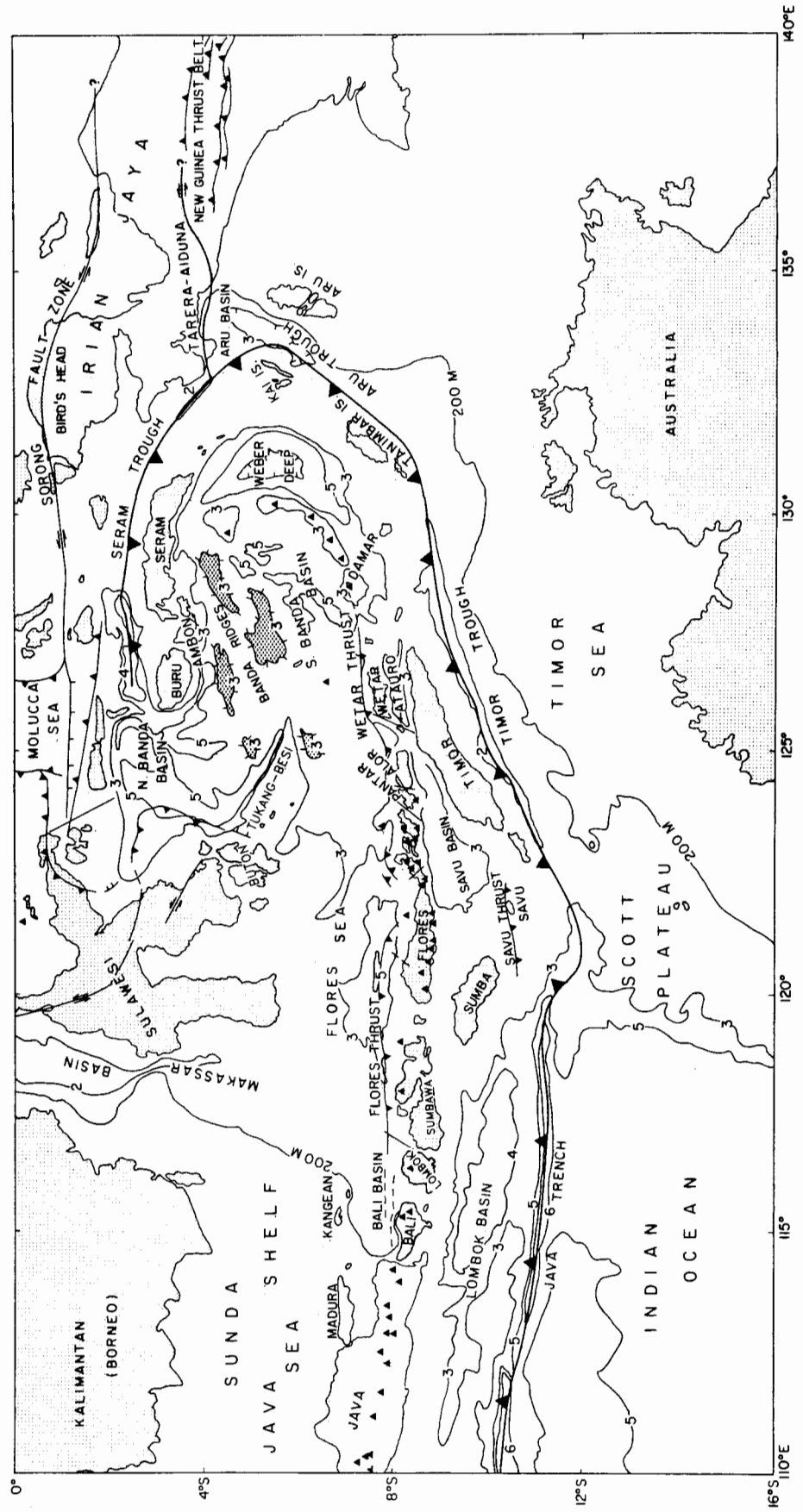

Fig. 1. Tectonic map of southeast Indonesia, modified from Hamilton [1979], Silver et al. [1983a,b,1986], and Silver [1981]. The Sunda arc extends from Java to Pantar, and the Banda arc stretches from Wetar to Ambon. Solid triangles show positions of active volcanoes [Simkin et al., 1981]. Bathymetric contours are labeled in kilometers, except the contour marked as 200 m. The cross-hatched areas are the portions of the Banda Ridges above 3 km water depth.

which 63 had long-period body waves large enough for analysis (Table 1). Some representative events are discussed in Appendix 1, and plots of solutions and waveforms for 50 events are in Appendix 3 on microfiche[1]. The remaining 13 have been published earlier (references in Table 1). The focus of this study is on the shallow earthquakes but because of possibly large errors in the reported depths, I examined all events whose depths as reported by the International Seismological Centre (ISC) place them in the upper 100 km. Fourteen of the events examined were found to be deeper than 40 km and likely occurred within the subducting Indian Ocean lithosphere [McCaffrey, 1988]. These events are described briefly in this paper insofar as they relate to the shallow tectonics. This study is limited to earthquakes arcward of the trenches; the reader should consult Cardwell and Isacks [1978], Fitch et al. [1981], and Dziewonski et al. [1981] for discussions of earthquakes at the Java trench, and analyses of earthquakes at the Seram trough and Aru Basin will be presented separately (no large earthquakes have occurred at the Timor and Aru troughs between 122°E and the Aru Basin).

The necessity of analyzing body waves is revealed by comparing depths determined from waveforms with those determined from travel times by the ISC. Referring to Figure 2, ISC depths based on P times can be shallower or deeper than those from waveforms; the mean difference (ISC depth minus waveform depth) is only 6 km, but the standard deviation is 25 km (52 comparisons). ISC depths based on what are identified as pP-P readings agree better with the waveforms for sources at depths in excess of 50 km, but shallower events still have large differences. Surprisingly, depths based on "pP-P" times are overestimated more consistently than those based on P times only; the difference is 27 ±24 km for 58 comparisons.

The waveform inversion method is one implemented on microcomputers by McCaffrey and Abers [1988] and is similar to that of Nabelek [1984] which is based on the teleseismic waveform modeling technique developed by Helmberger [1974] and Langston and Helmberger [1975]. Long-period teleseismic body waves from the World-Wide Standardized Seismograph Network (WWSSN) were hand-digitized, and for some events seismograms from the Global Digital Seismic Network (GDSN) were obtained. Typically, 10-30 seismograms are available for each event (Table 1). The double-couple point source is described by the strike ϕ and dip δ of one of the nodal planes, the rake angle λ on that surface [Aki and Richards, 1980], the centroid depth, and the amplitudes of the individual elements comprising the source time function. The source time function is represented by overlapping, triangular elements [Nabelek, 1985]. Solution parameter values are those that minimize the weighted sum of the squares of the residuals between the observed and calculated seismograms. Assumed source structures are based on published seismic refraction results (Appendix 2).

This paper examines the largest events between 1962 and 1984 in the overriding plate and therefore includes most of the seismic moment produced by earthquakes during that period. The seismic moments and fault plane solutions provide some sense of the distribution of strain for the region but must be interpreted with caution as these events may not truly represent the long-term regional strain for a number of reasons, two of which are the short sampling period and the unknown contribution of aseismic deformation. The long-term seismicity of eastern Indonesia is difficult to assess largely because the historical record is short. Nevertheless, compilations of seismicity for this century [e.g., Gutenberg and Richter, 1954; Duda, 1965] reveal a distribution of earthquakes that is similar to that of the 22 years examined here so that the relative importances of various modes of seismic deformation inferred from these earthquakes may be characteristic. However, it should be stressed that while the occurrence of earthquakes is a sign of active deformation, the lack of earthquakes on some feature does not mean that deformation does not occur. Clear examples of this are the Java trench and Timor trough, where any calculated seismic slip rate based on the earthquake history would most likely underestimate the true rate of subduction. While the earthquakes studied here reveal little about subduction of the Indian Ocean plate, they do demonstrate that some portion of the convergence is accommodated by shortening within the overriding plate, and this must be considered in tectonic models of the collision zone.

Where many earthquakes likely occurred on a single fault plane, such as on the Flores and Wetar thrusts, the slip rate v is calculated by

$$v = \frac{1}{Lwt} \sum_{q=1}^{N} \left[\frac{M_o}{\mu}\right]_q \qquad (1)$$

[Brune, 1968], where M_o is the seismic moment, L and w are the length and width of the fault surface, t is the time, the sum q is over the number of earthquakes N, and μ is the shear modulus ($\mu = \rho \cdot v_s^2$). Here w is taken to be the depth of the deepest earthquake divided by the sine of the dip angle of the fault; μ is inside the sum because different source densities and shear velocities were used to calculate the seismic moments for different earthquakes. Where earthquakes do not occur on a single fault, such as beneath the forearc and the Banda Basin, the analysis is more complicated as the rotational strain is likely to be significant and estimating it requires the difficult determination of which of the nodal planes is the fault plane [Molnar, 1983]. For these areas the elements of the symmetric moment tensor M_{ij} for each event are calculated [Aki and Richards, 1980; Kostrov, 1974] and summed (Table 2) in order to obtain some understanding of the overall deformation indicated by the earthquakes. The diagonal elements of the moment tensor do not depend on correct identification of the fault plane and are used to estimate the shortening or extension rates v_i in the upper plate using a modification of the method of Kostrov [1974]:

[1]Appendices 2 and 3 are available with entire article on microfiche. Order from American Geophysical Union, 2000 Florida Avenue, N. W., Washington, DC 20009. Document B88-020; $5.00. Payment must accompany order.

TABLE 1. Summary of Fault Plane Solutions

No.	Date	Origin time[a] UCT	Lat.[a] °S	Long.[a] °E	Depth,[b] km	M_b[a]	N[c]	Moment,[b] 10^{16} N m	Dur.,[d] s	ϕ,[b] deg	δ,[b] deg	λ,[b] deg	N.P.2[e] ϕ	N.P.2[e] δ	P axis Az	P axis Pl	T axis Az	T axis Pl	Num[f] P	Num[f] SH	Ref.[g]
1	May 15, 1962	0523:51.0	7.44	128.30	20.0±5.0	-	-	5000± 100	10	54±51	45± 3	90± 6	234	45	144	0	192	90	7	0	MN86
2	March 24, 1963	0207:08.0	9.70	120.54	25.4±1.2	-	-	328± 91	3	338± 4	50± 2	58± 3	202	49	90	0	181	66	10	3	
3	May 18, 1963	1220:31.5	8.21	115.55	16.0±1.0	-	-	43± 13	4	259± 2	76± 2	84± 5	102	15	354	31	161	59	13	11	MN87
4	May 22, 1963	2153:01.6	8.14	115.66	13.4±0.8	-	-	79± 15	3	266± 2	78± 2	83± 4	117	14	2	33	167	56	15	14	MN87
5	Sept. 4, 1964	1034:13.1	3.90	131.49	21.3±0.8	5.7	164	160± 10	3	332± 2	66± 1	59± 3	208	38	84	15	200	57	16	7	
6	May 31, 1965	1138:25.9	7.53	128.60	66.4±1.6	5.8	157	83± 76	6	246± 3	89± 3	271± 5	21	1	157	46	335	44	11	6	
7	April 21, 1967	0814:24.5	5.45	126.77	10.0±1.3	5.4	184	265± 110	9	235± 2	69± 3	21± 4	137	70	186	1	96	29	11	9	
8	April 22, 1967	0837:25.7	5.56	126.81	8.9±1.1	5.3	117	57± 11	4	278± 4	42± 2	70± 4	124	51	202	5	93	76	8	5	
9	Oct. 12, 1967	1831:39.0	7.15	129.83	91.2±0.9	6.0	252	140± 24	4	117± 3	51± 2	51± 4	349	53	53	1	322	61	13	5	
10	Jan. 26, 1968	0445:41.7	8.93	120.32	8.7±1.2	6.0	261	2012± 205	20	55± 2	84± 2	13± 2	324	77	189	5	280	13	16	0	
11	July 17, 1968	0524:15.2	8.66	125.03	5.5±1.0	5.6	183	103± 23	6	185± 4	57± 2	278± 4	351	34	120	77	269	12	11	3	
12	Feb. 24, 1969	0008:46.0	6.23	131.01	43.3±2.1	5.6	203	285± 117	6	156± 1	90± 1	208± 2	66	62	25	19	287	19	11	5	
13	Jan. 9, 1970	2316:20.6	9.27	117.25	64.6±0.7	5.7	194	66± 2	2	342± 3	69± 1	94± 4	151	21	69	24	259	66	16	9	
14	June 28, 1970	0130:13.8	8.75	124.04	80.0±1.0	6.2	333	1170± 167	8	59± 3	80± 2	95± 6	212	11	145	35	335	55	12	2	M85
15	Aug. 13, 1970	0422:35.3	9.00	117.95	95.8±1.2	5.9	290	74± 9	3	137± 5	47± 2	57± 5	1	52	70	3	333	66	11	7	
16	March 8, 1972	0345:25.1	3.74	131.39	27.5±1.2	5.9	243	92± 20	6	327± 4	67± 2	71± 5	188	30	71	20	206	63	13	12	
17	Sept. 11, 1972	1335:49.1	3.29	130.75	20.7±1.6	5.5	202	193± 37	14	307± 4	64± 1	79± 4	151	28	45	18	195	69	19	11	
18	Sept. 18, 1972	2035:35.5	9.93	119.60	58.9±0.9	5.8	181	28± 4	2	15± 3	69± 3	132± 4	127	46	76	14	330	48	8	2	
19	Sept. 24, 1972	2009:36.2	6.22	131.15	28.5±1.5	6.0	388	2018± 653	20	82± 2	54± 2	209± 2	334	67	293	44	31	8	18	10	
20	Oct. 17, 1972	2123:16.9	10.37	120.51	28.6±1.2	5.5	216	98± 30	5	103± 3	55± 1	83± 3	295	36	198	10	347	79	11	7	
21	Oct. 18, 1972	1818:25.5	8.59	124.93	19.5±1.2	5.7	218	87± 10	5	136± 5	81± 2	233± 6	34	38	11	42	254	27	11	6	
22	April 10, 1973	1955:53.5	9.81	119.29	65.0±0.9	5.8	254	51± 6	3	359± 4	46± 1	108± 3	154	47	256	0	348	77	11	5	
23	Dec. 19, 1973	0442:59.8	9.52	119.39	27.9±0.8	6.0	330	264± 44	4	92± 3	70± 2	95± 3	257	21	178	25	11	65	16	4	
24	March 6, 1974	1929:09.8	6.47	129.10	11.7±1.1	5.7	270	404± 83	3	311± 2	88± 2	174± 2	41	84	356	3	266	6	9	4	
25	July 26, 1974	1301:02.8	3.53	128.91	14.4±0.7	5.6	259	48± 2	2	135± 5	49± 1	93± 4	310	41	223	4	73	85	14	7	
26	Sept. 21, 1974	0313:01.4	6.39	129.07	11.4±2.0	5.3	188	37± 13	4	296± 4	60± 2	112± 5	77	37	10	12	249	67	9	8	
27	Dec. 3, 1974	0306:35.7	5.04	129.99	9.2±1.0	6.0	299	555± 33	5	58± 2	80± 3	358± 3	148	88	14	8	283	6	17	8	
28	Jan. 14, 1975	1937:18.1	4.93	130.03	10.6±0.8	5.6	238	205± 45	12	112± 4	54± 2	82± 4	305	37	208	9	350	79	17	8	
29	Jan. 14, 1975	1949:05.0	4.93	130.09	8.5±0.9	6.0	319	926± 143	9	130± 6	50± 2	85± 7	318	40	224	5	5	84	15	5	
30	July 30, 1975	0917:12.4	10.09	123.84	14.7±1.3	5.7	306	173± 46	6	44± 4	78± 2	8± 2	312	82	359	3	268	14	10	2	
31	Sept. 2, 1975	1531:58.9	10.13	121.70	7.8±2.7	5.9	277	47± 13	6	79± 9	45± 5	228±10	311	58	274	61	17	7	10	3	
32	Sept. 25, 1975	1234:07.3	7.24	127.97	10.6±1.3	5.5	150	30± 7	4	274± 4	48± 1	106± 4	71	44	353	2	254	78	8	7	
33	Dec. 30, 1975	0735:03.9	8.15	125.39	10.8±1.8	5.5	156	26± 8	4	71± 7	45± 2	103± 3	233	46	332	1	66	81	7	4	
34	March 3, 1976	2250:12.4	8.36	121.46	22.0±1.5	5.9	223	44± 21	4	252± 8	39± 3	93± 4	68	51	160	6	322	84	9	3	
35	July 14, 1976	0713:23.7	8.17	114.79	13.7±0.6	6.1	389	694± 42	3	279± 2	58± 1	87± 2	105	32	11	13	180	77	17	7	MN87
36	July 14, 1976	1023:46.8	8.15	114.79	9.6±0.6	5.9	292	42± 2	1	275± 2	58± 1	82± 2	110	33	11	13	162	76	8	6	MN87
37	Jan. 2, 1977	0955:29.3	10.16	119.03	15.7±1.1	5.7	297	293± 27	12	87± 2	76± 1	89± 3	271	14	178	31	356	59	19	6	
38	March 15, 1977	0855:00.5	4.96	131.03	11.0±2.1	5.8	291	65± 20	3	187± 4	68± 6	23± 8	88	69	138	0	47	31	8	9	
39	Aug. 27, 1977	0712:19.5	8.10	125.38	10.0±4.0	6.2	419	4110± 40	13	50± 4	39± 2	81± 2	242	52	326	6	189	82	15	4	MN86
40	Oct. 7, 1977	1210:43.3	9.99	117.29	15.7±1.5	5.9	334	399± 86	6	219± 3	75± 2	344± 3	313	74	176	22	266	1	18	7	
41	Feb. 12, 1978	0334:28.6	8.70	124.00	107.0±1.2	5.8	252	60± 13	4	70± 3	89± 3	99± 4	166	9	151	43	349	45	9	6	M85
42	March 27, 1978	1036:06.0	8.62	125.07	6.3±1.4	5.8	263	80± 13	3	185± 6	51± 2	262± 6	18	40	53	82	281	6	6	5	
43	Dec. 23, 1978	0510:47.2	8.27	121.38	11.4±0.8	5.8	226	183± 8	8	114± 9	30± 2	114± 6	267	63	7	17	150	69	10	0	MN84
44	May 21, 1979	1631:01.8	8.33	115.87	12.3±1.1	5.6	224	55± 13	3	265± 3	61± 2	69± 3	123	35	10	14	135	67	7	5	MN87
45	May 30, 1979	0938:55.3	8.31	115.86	11.0±0.5	6.0	337	236± 42	3	271± 1	61± 1	73± 1	123	33	13	14	146	69	19	5	MN87
46	Oct. 20, 1979	0141:10.3	8.38	115.87	13.7±0.6	5.9	360	487± 40	6	270± 2	63± 1	78± 2	115	29	9	17	155	70	20	8	MN87
47	Nov. 3, 1979	2317:37.8	4.26	129.74	6.1±1.3	5.7	211	94± 26	5	319± 5	44± 3	111± 7	111	50	214	3	315	75	12	7	
48	Dec. 17, 1979	1958:23.0	8.50	115.76	18.0±0.8	5.6	306	448± 55	5	260± 2	75± 1	70± 4	135	25	6	27	145	56	18	10	MN87

49	May 15, 1980	1858:29.3	6.16	125.72	7.0±0.9	5.7	309	401±	26	7	45± 3	76± 7	16± 6	311	75	178	1	269	21	14	8
50	May 22, 1981	0255:22.3	6.56	132.26	65.3±1.4	5.7	373	141±	6	2	81± 2	61± 3	15± 3	344	77	35	11	299	30	9	7
51	Sept. 17, 1981	0619:08.8	6.49	127.93	14.8±0.6	5.7	239	161±	6	2	54± 2	81± 2	1± 1	324	89	9	6	279	7	9	9
52a	March 11, 1982	1032:27.1	9.27	118.48	23.2±1.7	6.0	438	168±	34	6	178± 5	58± 3	336± 3	281	70	143	38	47	8	14	10
52b	March 11, 1982	1032:31.3	9.27	118.48	27.9±0.6	6.0	438	296±	93	6	201± 1	75± 1	357± 1	292	87	157	13	65	8	14	10
53	May 11, 1982	2046:59.5	7.71	128.45	57.1±1.7	5.6	256	27±	5	2	268± 4	75± 3	241± 5	153	32	145	51	20	24	5	5
54	Aug. 6, 1982	2040:51.6	8.50	120.55	15.3±1.0	5.5	205	40±	3	4	61± 3	69± 2	347± 3	156	78	20	24	287	6	9	9
55	Nov. 14, 1982	1623:57.3	9.52	122.58	60.3±1.3	5.6	237	21±	2	3	301± 5	54± 2	282± 4	101	38	254	77	22	8	8	7
56	Dec. 25, 1982	1228:01.9	8.43	123.18	7.1±1.0	5.5	211	94±	10	5	278± 2	85± 3	205±10	186	65	145	21	49	14	14	10
57	March 12, 1983	0053:40.2	4.04	127.89	11.5±1.0	5.8	337	154±	39	5	98± 5	42± 2	69± 5	305	51	23	5	274	75	11	6
58	March 12, 1983	0136:35.8	4.06	127.92	11.3±1.3	5.9	416	1026±	215	11	86± 5	65± 3	65± 4	314	35	194	16	317	62	14	7
59	July 24, 1983	2338:09.8	8.14	119.50	25.9±1.8	5.7	232	149±	64	4	258± 3	72± 2	80± 5	108	21	356	26	153	62	11	9
60	Oct. 31, 1983	1737:56.2	9.02	119.18	78.7±1.3	6.0	407	291±	63	8	296± 2	84± 2	64± 3	194	27	48	34	180	45	14	6
61	Nov. 20, 1983	2032:20.5	7.45	130.65	69.6±2.3	5.9	343	113±	49	3	75± 4	65± 4	18± 4	337	74	28	6	294	30	7	7
62	June 6, 1984	0538:23.6	4.82	125.85	7.7±1.6	5.9	234	182±	89	4	152± 2	90± 2	183± 3	62	87	17	2	287	2	11	7
63	Oct. 4, 1984	1631:53.4	9.81	118.79	18.6±1.7	5.7	367	260±	47	12	82± 3	73± 2	90± 5	262	17	172	28	352	62	10	10

[a]Lat., latitude; Long., longitude; Dur., source duration; Az, azimuth; Pl, plunge.
[b]Taken from ISC.
[c]Uncertainties are 2 standard deviations.
[d]The number of stations used in the ISC location.
[e]Time during which 95% of moment occurs.
[f]Strike and dip of nodal plane 2.
[g]Number of weighted P and SH waves used in the solution.
MN84, McCaffrey and Nabelek [1984]; M85, McCaffrey et al. [1985]; MN86, McCaffrey and Nabelek [1986]; MN87, McCaffrey and Nabelek [1987].

Fig. 2. Plots of the depths reported by the ISC versus those determined here by waveform modeling. Error bars are those given in the ISC bulletins for P and pP-P depths and a formal uncertainty of 5 standard deviations is shown for the waveform depths. The dashed lines are where the two depths agree.

$$v_i = \frac{\ell_i}{2Vt} \sum_{q=1}^{N} \left[\frac{M_{ii}}{\mu} \right]_q \qquad (2)$$

where ℓ_i is the length of the region in the ith direction (the i directions are north n, east e, and down z) and V ($=\ell_n\ell_e\ell_z$) is the volume of the region.

The formal uncertainties in the source parameters determined by the inversion routine underestimate the true uncertainties. When only a few earthquakes are examined the uncertainties can be estimated for each event by examining the fits to the observed seismograms while varying each parameter individually [e.g., Abers and McCaffrey, 1988; McCaffrey and Nabelek, 1986, 1987; Nabelek, 1984; Nelson et al., 1987; Stein and Wiens, 1986]. This approach is impractical for the large number of events studied here so the uncertainties are estimated in the following ways: (1) 26 waveform solutions are compared to published centroid moment tensor (CMT) solutions (Appendix 1); (2) for two representative events, subsets of the available seismograms are inverted to examine the effects of variations in the numbers and distributions of seismograms used (Appendix 2); and (3) synthetic seismograms for known sources are contaminated by various forms of noise and

TABLE 2. Composite Moment Tensors for Forearc and Back Arc Earthquakes

	P Axis Azimuth	M_{nn}	M_{ee}	M_{zz}	M_{ne}	M_{nz}	M_{ez}
Forearc	2°	-2.63	2.89	-0.26	-0.14	0.51	-0.57
Banda Basin	15°	-3.53	1.24	2.29	-1.39	0.70	-0.36

Forearc earthquakes are events 10, 11, 21, 30, 31, 40, 42, 52, 54, and 56. Banda Basin earth-quakes are events 7, 8, 24-29, 47, 49, 51, 57, 58, and 62. P axis azimuth is the azimuth of the P axis calculated from the composite moment tensor. M_{ij} is in units of 10^{19} N m and negative values indicate compression.

inverted while varying fixed parameters (Appendix 2). These tests indicate that uncertainties of 5 km in depth, 15° in strike, 10° in dip, and 20° in the rake angle are typical. The agreement of the double couples with the CMT solutions is particularly impressive (Appendix 1).

Source finiteness was ignored generally, but some waveforms displayed features that a point source could not reproduce. In such cases I tried multiple sources, each of which were allowed to vary in orientation and hypocenter, and experimented with directivity resulting from a horizontally rupturing line source. In all but one case (shown in Appendix 1) the improvements to the fits were not impressive enough to claim that such details were resolved, nor did the resulting changes in the source mechanisms affect the tectonic conclusions. Furthermore, tests in which synthetic seismograms generated for finite faults were used to determine the parameters of a point source show that the point source reasonably describes the average of the finite fault (Appendix 2 and Nabelek [1984]) when the source durations are short (less than 10 s).

Results and Interpretation

In this section the events are divided into tectonic subregions, and the tectonic implications for these subregions are discussed. The next section is a more interpretive discussion of the results in a regional context. The forearc is taken to be between the trenches (the Java trench and the Timor, Aru, and Seram troughs) and the volcanic arc, while the back arc is on the Banda Basin side of the arc. This division breaks down south of Seram because the Banda Ridges abut the forearc (Seram) and there is no clear volcanic arc, except near Ambon. Hence earthquakes south of Seram and Buru will be grouped with the back arc

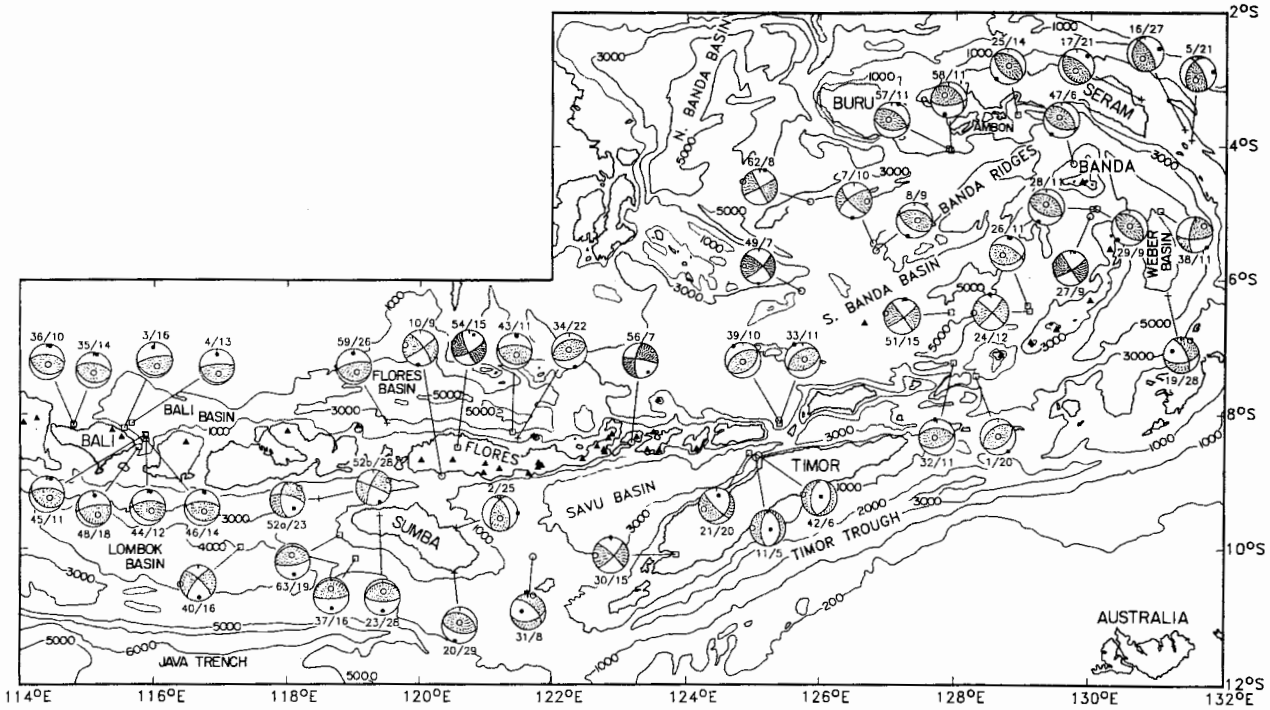

Fig. 3. Fault plane solutions for shallow (depth ≤ 30 km) earthquakes. Bathymetric contours [from Mammerickx, 1976] are labeled in meters. Labels beside focal spheres indicate the event number and depth (in kilometers) separated by a slash. Compressional quadrants of the lower hemisphere projections are stippled, and the dots and circles represent the P and T axes, respectively.

events. Earthquakes at depths greater than 40 km and some shallower events probably occurred within the subducting plate.

Interplate Underthrusting Earthquakes

Sumba. Three interplate earthquakes (23, 37 and 63) beneath Sumba Island at 16 to 28 km depth (Figures 3 and 4) indicate relative motion between the Indian Ocean plate and the island arc. Presumably the gently north dipping plane is the fault plane for these events, so that the slip vectors indicate a relative convergence direction of 357°±5°.

To my knowledge only one interplate underthrusting earthquake mechanism (May 1, 1978) has been determined for the Timor trough [McCaffrey, 1988]. While the mechanism is certainly a thrust, the event is quite small ($M_o \approx 10^{17}$ N m), and the orientation of the slip vector is too poorly constrained to provide constraints on the plate convergence direction near Timor.

Seram Trough. Underthrusting mechanisms were determined for three earthquakes (5, 16, and 17) at 21-27 km depth east of Seram. Slip vectors indicate thrusting of the Bird's Head beneath the Seram trough at an azimuth of 232°±15°. The azimuths of the slip vectors decrease from 242° for event 5 in the east to 237° for event 16 to 217° for event 17 in the west, consistent with a Bird's Head-Seram rotation pole to the SE of these events, near the Aru Basin. The three earthquakes had a total moment of $4.5\pm0.3\times10^{18}$ N m; using (1) and L=350 km, w=27 km/sin(20°)=79 km, and t=22 years, the slip rate is a mere 0.2±0.1 mm/yr.

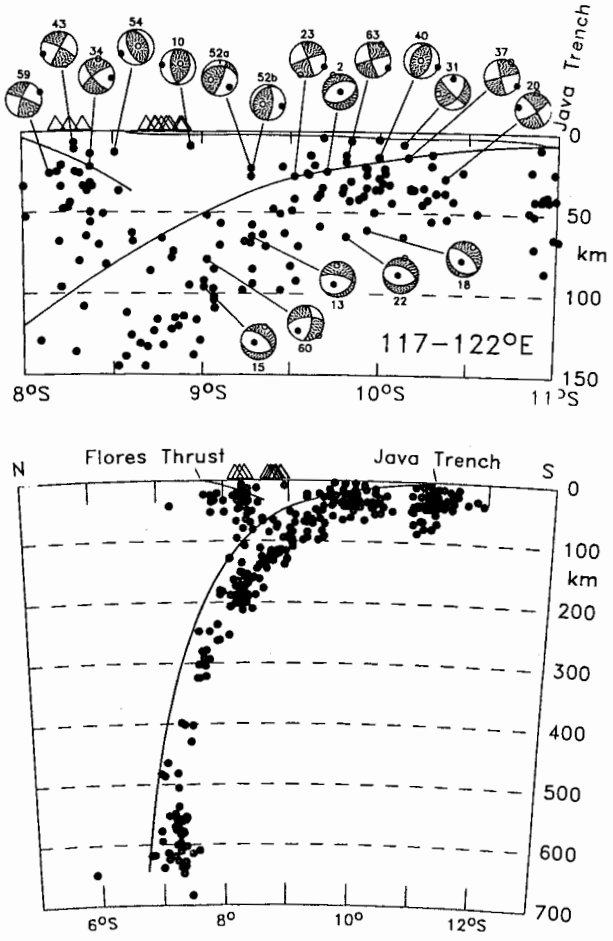

Fig. 4. North-south cross sections of earthquake hypocenters and fault plane solutions in the vicinity of Sumba Island, from 117° to 122°E. Focal mechanisms are labeled by event number. Compressional quadrants for the side hemisphere projections are stippled, and the dots and circles represent the P and T axes, respectively. Triangles show positions of active volcanoes. The inferred top of the subducting plate (heavy line) is defined in the upper 30 km by underthrust events 23, 63, and 37 and deeper by the upper envelope of the seismic zone defined by hypocenters (dots) in the lower plot. Average bathymetry is shown by the lighter line. Hypocenters shown are selected from the ISC lists as described by McCaffrey [1988]. No vertical exaggeration.

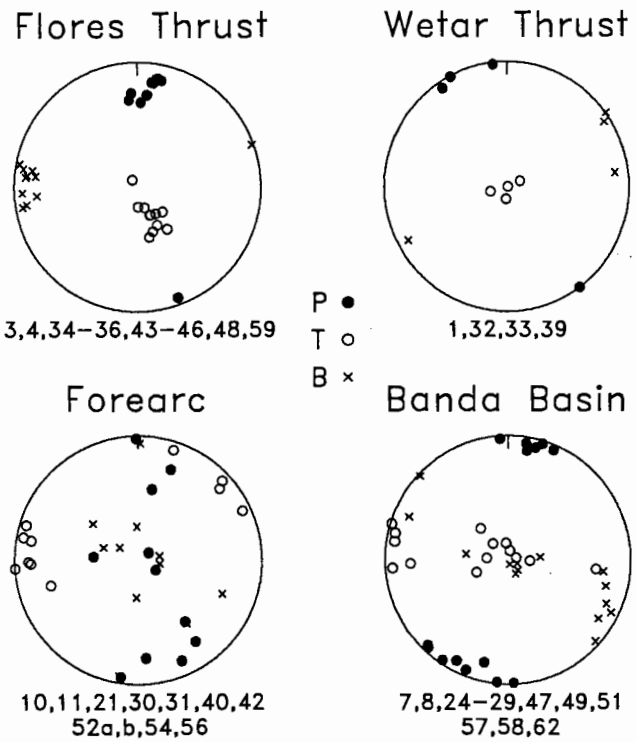

Fig. 5. Lower hemisphere projections of P, T, and B axes inferred from fault plane solutions. Events are separated by tectonic region as labeled. Numbers beneath each sphere indicate the events plotted.

Forearc Upper Plate Earthquakes

Sumbawa to Timor. Shallow earthquakes in the upper plate beneath the arc and forearc show strike-slip (10, 30, 40, 52, 54, and 56) and normal (11, 21, 31, and 42) faulting. Event 40, beneath the Lombok Basin, is the largest strike-slip aftershock associated with the great Sumba earthquake of 1977.

Fault plane solutions for earthquakes in the forearc and arc, excluding events 2 and 31 beneath the Savu Basin, reveal a consistent orientation of the T axes in an east to ENE direction (Figure 5). The P and B axes tend to group together, indicating that the maximum and intermediate compres-

sive stresses are similar in magnitude and oriented vertically or north to NNW. The predominant deformation modes for the arc and forearc are therefore E-W extension (positive M_{ee}; Table 2) and N-S shortening (negative M_{nn}) and are interpreted to be a response to the encroachment of the Australian continent. Using (2) and ℓ_n=300 km, ℓ_e=1000 km, ℓ_z=20 km, and t=22 years, the rate of N-S shortening in the forearc is 0.8±0.4 mm/yr while E-W extension is 2.9±1.5 mm/yr.

Earthquakes in the upper plate beneath Timor reveal strike-slip and normal faulting mechanisms (events 11, 21, 30, and 42; Figure 3). Although crustal thickening has probably played an important role in the development of the forearc at Timor, earthquakes suggest that it is now of minor importance (small M_{zz}), though it may occur aseismically.

Savu Basin. The Savu Basin is a triangular forearc basin between the volcanic arc and the islands of Timor, Savu, and Sumba (Figure 1). The basin contains >2 km of sedimentary fill and east trending buried basement ridges, of unknown origin, west of 122.5°E that bend to a NE trend in the eastern part [Karig et al., 1987]. Two earthquakes beneath the Savu Basin do not fit the pattern of the remainder of the forearc. Event 2, at 25 km depth, is similar to deeper events in the slab and may have occurred in the slab (Figure 4). Event 31, at 8 km depth, shows N-S extension in the southern Savu Basin midway between a pair of east trending buried ridges (the South Sumba arch and North Sumba ridge of Karig et al. [1987]). Its mechanism is very similar to one for a different earthquake at the same location determined by McCaffrey et al. [1985, mechanism 22]. I found no earthquakes on the Savu thrust [Silver et al., 1983a].

Event 20. The mechanism of this earthquake differs from the underthrusting events in that its north dipping nodal plane is steeper than those of events 23, 37, and 63 (36° compared to 21°, 14°, and 17°). While it seems to fall beneath the top of the subducting plate in a north trending projection (Figure 4), if the plate's depth contours swung to the SW from event 23 parallel to the long axis of Sumba and to the Java trench (Figure 3), it would be at the top of the plate and indicate a more NNE direction of subduction. If it does occur within beneath the plate interface, it could be due to faulting within the subducting plate during subduction or it may be a compressional bending event below the neutral fiber of the bent plate (it is located less than 200 km NE of the epicenter of the great Sumba normal-faulting event of 1977).

Weber Basin. The Weber Basin, called the Weber Deep at its deepest part, is an unusually deep forearc basin, reaching depths in excess of 7.5 km, roughly twice the depth of its associated trench (the Aru trough; Figures 1 and 6). It is underlain by oceanic crust, has a thin sedimentary cover, and is associated with a large, negative free-air gravity anomaly (<-300 mGal) that can be explained by 2-4 km of subsidence of oceanic crust that was originally in isostatic equilibrium [Bowin et al., 1980].

Explanations for the great depth of the Weber Basin include the following: it is the subduction trench at the eastern end of the Banda Arc [e.g., Audley-Charles and Milsom, 1974]; it is the

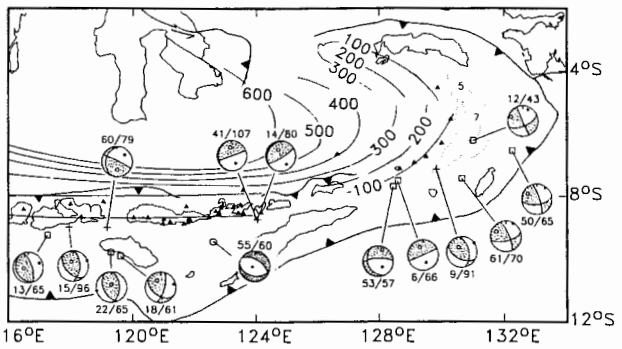

Fig. 6. Fault plane solutions for events deeper than 40 km. Labels beside focal spheres indicate the event number and depth (in kilometers) separated by a slash. Compressional quadrants of the lower hemisphere projections are stippled, and the dots and circles represent the P and T axes, respectively. The dotted lines show the 5- and 7-km contours of the Weber Basin. The thin curved lines are the contours of the top of the seismic zone determined by McCaffrey [1988] and labeled in kilometers.

elastic response of the lithosphere to uplift of the leading edge of the forearc that had continental crust and sediments stuffed beneath it [Hamilton, 1979]; it is the elastic response to the curvature of the Banda arc [Bowin et al., 1980]; and the slab below it has detached and the basin is being pulled down by mantle flow [Bowin et al., 1980]. Shallow earthquakes (19 and 38) at 28 and 11 km depth, respectively, beneath the basin show strike-slip faulting and epicenters extend well east of the Weber Basin (Figures 3 and 7), both inconsistent with the subduction zone hypothesis. The details of the flexural models of Hamilton [1979] and Bowin et al. [1980] are not clear; nevertheless, it is likely that elastic stress large enough to depress the lithosphere of a 120-km-wide basin by 2-4 km would produce some observable effects elsewhere, in particular, uplift and gravity anomalies. The detached slab model is unlikely because there is seismic activity in the upper mantle beneath the basin (Figure 7).

On the basis of the depths and mechanisms of the earthquakes I propose instead that the crust and upper mantle of the Weber Basin sits directly on the subducting lithosphere so that its vertical motions are simply adjustments to the vertical motions of the sinking lithosphere. Event 12 is at 43 km depth beneath the Weber Basin, and its fault plane solution is virtually identical to other deeper events from the eastern Banda forearc that clearly occurred within the subducting lithosphere (events 50 and 61 at 65 and 70 km depth, respectively; Figures 6 and 7). Event 19, at 28 km depth, occurred near event 12 but with a much different mechanism; its mechanism is, however, similar to that of event 38 beneath the northern Weber Basin at 11 km depth (Figure 3). From the difference in mechanisms for events above and below 40 km depth, I infer that event 12 occurred within the lower plate and event 19 occurred within the overriding plate. Accordingly, the top of the downgoing plate (Figure 7) must fall

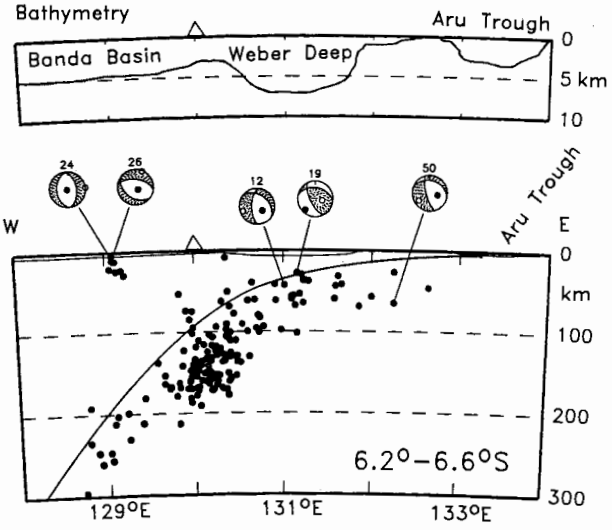

Fig. 7. Cross sections of fault plane solutions in an E-W profile across the Weber Basin from 6.2° to 6.6°S (format as in Figure 4). The top of the seismic zone is constrained to pass between the hypocenters of events 12 and 19 and to form an upper envelope for the ISC hypocenters deeper than 100 km. The top plot shows the bathymetry along the same profile at 10× vertical exaggeration.

between the hypocenters of the two events and is consistent with the ISC hypocenters in that it roughly forms an upper envelope for them. If this reasoning is correct, then the top of the subducting plate is no deeper than 40 km beneath the Weber Basin.

The Moho depth beneath the central Weber Basin is 18-21 km, and the upper mantle P wave velocity is 7.8-7.9 km/s [Bowin et al., 1980]. Earthquake 19, at 28 km depth, occurred within the upper mantle beneath the basin, indicating that the mantle there behaves brittlely, despite its relatively low seismic velocity which would otherwise imply high temperatures. The shallowness of the subducting plate beneath the Weber Basin and the presence of seismic activity in the upper mantle both suggest that there is probably not an asthenospheric wedge between the upper and lower plates beneath the Weber Basin. If this is correct, then the vertical motion of the upper plate will be identical to that of the subducting plate since isostatic compensation requires a substrate which behaves as a fluid on the appropriate time scale and the uppermost part of the subducting plate probably does not have such behavior.

As noted above, the Weber Basin is an unusually deep forearc basin and is well out of isostatic equilibrium. Its nonisostatic subsidence is probably a consequence of subduction of continental crust at the Aru trough. When continental crust enters the trench, its buoyancy likely causes subduction to slow. In response to the change in plate velocity at the trench, the subducted slab can either detach near the surface and continue sinking along the same trajectory, or if it remains attached to the surface part of the plate, as is likely the case here, it must define a new trajectory. In the latter case the new path will be deeper than the old path (relative to the overriding plate), and because the old and new trajectories coincide at the trench, the vertical difference between the two paths will increase from the trench toward the volcanic arc [e.g., Turcotte and Schubert, 1982]. If the lithosphere of the forearc basin sits directly on the subducting plate, as earthquakes suggest for the Weber Basin, then it will sink as the subducting plate drops from under it.

Back arc Thrusting

Thrusting north of the volcanic arc at the southern edges of the Bali, Flores, and Banda basins is evident in seismic reflection profiles [Hamilton, 1979; Silver et al., 1983a; Usna et al., 1979], SeaMARC profiling [Silver et al., 1986], and in the presence of thrust earthquakes and gravity anomalies [McCaffrey and Nabelek, 1984, 1986, 1987]. The thrust zones accommodate southward thrusting of the back arc basin beneath the volcanic islands in a sense opposite to subduction at the Java trench and Timor trough.

Flores thrust. The Flores thrust zone extends from the Bali Basin to north of central Flores (Figure 1). Eleven thrust earthquakes occurred on the Flores thrust zone, eight of which occurred beneath the Bali Basin (events 3, 4, 35, 36, 44-46, and 48) and have been discussed by McCaffrey and Nabelek [1987]. Slip vectors for the 11 earthquakes indicate convergence between the back arc basin and the island arc at an azimuth of 176° ± 8°. The earthquakes produced a total seismic moment of $2.46\pm0.16\times10^{19}$ N m. Using (1) and L=720 km, w=26 km/sin(30°) = 52 km, and t=22 years, the seismic slip rate for the Flores thrust is 0.8±0.1 mm/yr.

The Flores thrust zone is morphologically the most mature of the back arc thrust zones, and the amount of shortening estimated from the volume of accreted sediments is at most 60 km [Silver et al., 1983a]. Although the ISC hypocenters appear to define a seismic zone that dips southward from the Flores thrust to nearly 100 km depth (Figure 4), the depths of these earthquakes are not reliable enough to justify such an interpretation. The deepest earthquake found from the waveform analysis is at only 26 km depth (event 59). The size of the uncertainties in the ISC depths (Figure 2) are such that all events in the apparent south dipping zone may in fact be shallower than 30 km. Thus, while thrusting likely penetrates the upper mantle, the lack of conclusive evidence for deeper earthquakes leaves the question of subduction polarity reversal unresolved. Moreover, the reaction of the Banda Basin to collision with Australia (discussed below) demonstrates that subduction polarity reversal is not the only possible outcome of arc-continent collision. The presence of a well-developed thrust zone in the back arc basin, particularly north of Flores, is not by itself sufficient evidence that polarity reversal will occur. A possible analogy, in my opinion, of a back arc thrust zone that resulted from arc-continent collision but was subsequently abandoned is the New Guinea trench.

Wetar Thrust. The Wetar thrust zone extends from eastern Alor nearly to Damar (Figure 1). The total amount of convergence is much less than on the Flores thrust, probably less than 10 km

[McCaffrey and Nabelek, 1986]. Four thrust earthquakes (events 1, 32, 33, and 39) with nodal planes dipping at roughly 45° to the NW and SE were located along the Wetar thrust zone. These included the two largest earthquakes examined (events 1 and 39). Events 33 and 39 reveal a more NW direction of convergence (140°-150°) on the western end of the Wetar thrust than on the Flores thrust (Figure 3). Using (1) and L=450 km, w=20 km/sin(45°)=28 km, ΣM_o=9.17±0.16×10^{19} N m, and t=22 years, the seismic slip rate for the Wetar thrust is 8.8±0.2 mm/yr.

Ambon Thrust. Three, and possibly four, thrust earthquakes suggest the presence of a thrust zone south of Ambon and Seram (Figure 3) that I call the Ambon thrust. Earthquakes 25, 57, and 58 occurred at the base of the back arc slope of Ambon and Seram and in this sense are similar to those on the Flores and Wetar thrusts. They show north to NE directed thrusting. Event 58, the sixth largest event examined, produced a tsunami on Seram [Lockridge and Smith, 1984], indicating a shallow source. Thrusting south of Seram moves it SW with respect to the Banda Basin, but the fault planes for these earthquakes cannot be identified. Seismic profiles over the epicentral region of events 57 and 58 reveal deformation in the sediments, but the sense of displacement and the amount of shortening are not evident [Usna et al., 1979; E.A. Silver, unpublished data, 1981].

Banda Basin

The Banda Basin comprises two deep-water basins, the North and South Banda basins, separated by a NE trending series of basins and ridges called the Banda Ridges (Figures 1 and 3) and by the Tukang Besi platform that extends southeastward from SE Sulawesi [Silver et al., 1983b, 1985]. The Banda Ridges generally rise to bathymetric depths of less than 2 km and are locally emergent, while intervening basins are in excess of 5 km deep. Dredge hauls from the Banda Ridges reveal continental clastic sedimentary and metamorphic rocks with strong similarities in age and lithology to those on the neighboring islands and in Irian Jaya. The ridges are probably slivers of the Bird's Head of New Guinea detached between 5 and 10 Ma [Silver et al., 1985]. The ages of the North and South Banda basins are unknown.

Earthquakes beneath the Banda Basin are predominantly thrust (events 8, 26, 28, and 29) and strike slip (events 7, 24, 27, 49, 51, and 62). Despite the different locations and mechanisms, P axes for these events are aligned similarly (Figure 5). The composite moment tensor reveals strong components of N-S shortening (negative M_{nn}; Table 2) and crustal thickening (positive M_{zz}), with a smaller amount of E-W elongation (positive M_{ee}). Using (2) and ℓ_n=450 km, ℓ_e=450 km, and ℓ_z=15 km the rate of N-S shortening in the back arc basin is 3.2±1.6 mm/yr and the rate of E-W extension is 1.2±0.6 mm/yr. The azimuth of the P axis defined by the composite moment tensor is 15° (Table 2), which is slightly to the NNE of that within the forearc but still likely reflecting the collision of the arc with Australia.

Earthquakes in the Banda Basin occur primarily within the Banda Ridges south of Seram and at the southern and eastern edges of the South Banda Basin (Figure 3). Event 49 occurred at 7 km depth 40 km SW of a NW trending bathymetric low bordering the Tukang Besi Plateau on the NE (Figure 8). This feature, named the Hamilton fault by Silver et al. [1985], was labeled a "possible inactive trench" by Hamilton [1979, Figure 76C]. The mechanism of event 49 shows that it may be associated with strike-slip faulting. Event 62 occurred near the northern border of the Banda Ridges, probably on a NE trending bounding fault. If so, it shows left-lateral motion between the North Banda Basin and the Banda Ridges.

Beneath the eastern margin of the South Banda Basin and west of the volcanic arc, a mix of strike-slip and thrust earthquakes are found (Figure 3). The deepest of these is event 51, a strike-slip earthquake at 15 km depth, and it is also beneath the deepest part of the South Banda Basin. Despite the change in structural trend to N-S at the eastern end of the volcanic chain, the P axes maintain a north to NNE trend, suggesting that the mechanisms are reliable indicators of the direction of maximum compressive stress within the crust of the Banda Basin. It follows that the maximum compressive stress, which presumably arises from collision with Australia, is greater in magnitude than the horizontal deviatoric stress in the crust generated by changes in the topography. Such stress can be several tens of megapascals in the direction perpendicular to the trend of the topography [e.g., Dalmayrac and Molnar, 1981; Turcotte and Schubert, 1982].

While such topographic stress is apparently not large enough to affect observably the direction of the maximum compressive stress, it may affect the intermediate and least compressive stress directions. T and B axes of earthquakes in the Banda Basin tend to be either vertical or horizontal and tend to cluster (Figure 5) suggesting that the intermediate and least compressive stresses are similar in magnitude (i.e., $\sigma_n \gg \sigma_e \approx \sigma_z$ where σ is the principal stress in the direction n, north; e, east; or z, down). If the increase in the E-W compressive stress σ_t that results from N-S striking bathymetric features of the eastern Banda Basin is large enough to cause the least compressive stress, which is horizontal for strike-slip faulting ($\sigma_n \gg \sigma_z > \sigma_e$), to become larger than the intermediate stress (i.e., $\sigma_n \gg \sigma_e + \sigma_t > \sigma_z$), the B and T axes will swap and thrust faulting will occur instead of strike slip. While this mechanism can account for the presence of both strike-slip and thrust faulting under constant regional stress in the Banda Basin, it cannot be tested by these data because of the large uncertainties in both the earthquake locations and bathymetry.

There is a temporal relationship between some thrust and strike-slip events in that thrust events often occur shortly after strike-slip events and in the same region. For example, events 7 and 8 were 1 day apart, and events 24 and 26 were 6 months apart (Figure 3 and Table 1). Event 27 was followed in a month by two thrust events (events 28 and 29). The strike-slip earthquakes may perturb the stress field locally to cause the thrust faulting, although the occurrence of isolated thrust events indicates that a large strike-slip event is not a necessary condition for thrusting.

Lower Plate Earthquakes

Fourteen earthquakes at depths greater than 40 km beneath the forearc likely occurred within the subducting plate (Figure 6). Two others at shallower depths fall near the inferred plate

interface (events 2 and 20; see Figure 4) so it is not clear whether they occurred above or below it. Several events (9, 12, 13, 15, 18, 22, 50, 61, and possibly 2) display nearly horizontal P axes that are parallel to the local strike of the slab while their T axes plunge in the downdip direction of the slab. These have been explained by cross-slab compression caused by the bend in the subducted slab at the eastern end of the arc [Cardwell and Isacks, 1978; Fitch and Molnar, 1970]. Other events (6, 14, 41, and 53) have one nodal plane that strikes parallel to the slab and dips steeply with T axes also plunging to the north to NNW. These have been interpreted as evidence that the lower part of the slab is detaching from the upper part [McCaffrey et al., 1985; Osada and Abe, 1981]. Interpretation of these earthquakes in relation to the subducting slabs is given by McCaffrey [1988].

Interpretation of the Active Tectonics of the Collision Zone

The relative motion between SE Indonesia, at the southeastern edge of Southeast Asia (SEA), and the surrounding plates is not constrained well, owing particularly to complex deformation within Asia and Indonesia. Slip vectors for underthrusting earthquakes south of Java [Cardwell et al., 1981; Kappel, 1980], beneath Sumba, and along the Flores thrust zone (Figure 3) indicate a 0°-10° convergence direction between the Indian Ocean, the eastern Sunda arc, and the Sunda Shelf (which is part of SEA). Both the Minster and Jordan [1978] solution and the presence of a long seismic zone [Cardwell and Isacks, 1978; Hamilton, 1974; McCaffrey, 1988] in ≈150 Ma subducting oceanic lithosphere [Larson, 1975] suggests that the overall convergence rate near Sumba and Timor is probably 70-80 mm/yr [Molnar et al., 1979]. In the northern Banda arc the Pacific plate moves at an azimuth of 283° and rate of 97 mm/yr with respect to Eurasia [Minster and Jordan, 1978], although motion of the Philippine Sea plate and deformation within Asia add some uncertainty to these numbers.

Cardwell and Isacks [1978] inferred from the shape of the subducted lithosphere beneath the Banda Sea that the relative motion between the Banda arc and Australia has been NNW over the past few million years. Because of the discrepancy with the Minster and Jordan [1978] predicted convergence direction, 20°, they suggested that SEA is not part of the Eurasian plate, and Johnston and Bowin [1981] went on to suggest that SEA is moving eastward at 60 mm/yr relative to the Eurasian plate. I suggest that the apparent eastward motion of the Banda arc with respect to Eurasia can be explained by deformation in the Banda Basin, Banda arc, and eastern end of the Sunda arc. Eastward migration of the Banda arc was proposed by Hamilton [1977], but in his model it was driven by back arc spreading in the Banda Basin. In my view this migration is caused by strike-slip faulting that accompanies the predominantly N-S shortening due to collision.

Shallow earthquakes show that the present stage of the collision of Australia with the Banda arc proceeds by convergence distributed over the entire forearc, island arc, and back arc basin rather than only at the Timor and Seram troughs. Convergence in the upper plate is manifested by a combination of thrust faulting that shortens the back arc basin in a N-S direction and thickens its crust and by strike-slip faulting that shortens the forearc, arc, and back arc basin in a N-S direction while elongating them in the E-W direction.

Seismic moments of earthquakes from the upper plate at the Banda arc can account for approximately 12 mm/yr of convergence between the Australian continent in the south and Seram in the north for the past 22 years: approximately one-fifth of the expected total convergence rate for Australia and SE Indonesia. Along the Sunda arc to the west, N-S shortening is much slower (the forearc and Flores thrust combine for only ≈2 mm/yr). The forearc and the Banda Basin both show slow E-W extension. I interpret fault plane solutions as showing that the forearc undergoes left-lateral N-S shear so that both Timor and the Timor trough have a northward component of motion with respect to the Sunda arc to the west, resulting in counterclockwise rotation of the eastern Sunda and southern Banda forearcs. Such rotation can only be inferred from the strike-slip fault plane solutions because it depends on which of the nodal planes is the fault plane but, it is consistent with the eastward increase in the amount of N-S shortening that occurs in the overriding plate.

An interpretation of the present deformation in the eastern Sunda and Banda arcs is depicted by several independent crustal blocks (microplates) in Figure 8. Because of the limited number of earthquake mechanisms, it is not clear whether the region actually consists of separate rigid blocks as shown or if it would be characterized better by plastic deformation. The treatment here in terms of discrete fault-bound blocks is largely for description, although the recognition of faults in Timor (T. Charlton and A. Barber, unpublished manuscript, 1987) and the lithologic and structural contrasts between the Banda Basins and Banda Ridges [Silver et al., 1985] support the microplate approach. The faults shown by dashed lines are admittedly speculative and may in fact have a very different geometry. Some of the blocks are clearly being disrupted internally and note is made of such behavior.

Eastern Sunda arc. Over the past 25 years, thrust earthquakes along the Java trench east of Sumatra and west of the Savu Basin have been rare and small; the largest are about magnitude 6 [Kappel, 1980] with a seismic moment of less than 3×10^{18} N m (events 23 and 37, Table 1). The historical record also reveals few large earthquakes that could be interpreted as interplate events beneath the forearc south of Java [Kelleher and McCann, 1976; Newcomb and McCann, 1987]. East of the Savu Basin, only one underthrusting earthquake has been found beneath the forearc north of the Timor trough, and this was fairly small [McCaffrey, 1988]. Evidence of large, active, continuous thrust zones that would indicate closure of the forearc in response to the collision is lacking in seismic profiles [e.g., Karig et al., 1987; Silver et al., 1983a]. This study shows that shallow earthquakes beneath the forearc and arc are typically strike slip and are larger than the thrust events; the three largest forearc events show strike-slip faulting. I infer that strike-slip motion plays an important role in the deformation of the arc during collision.

The slip direction on the Flores thrust zone is the same as that between the Indian Ocean plate

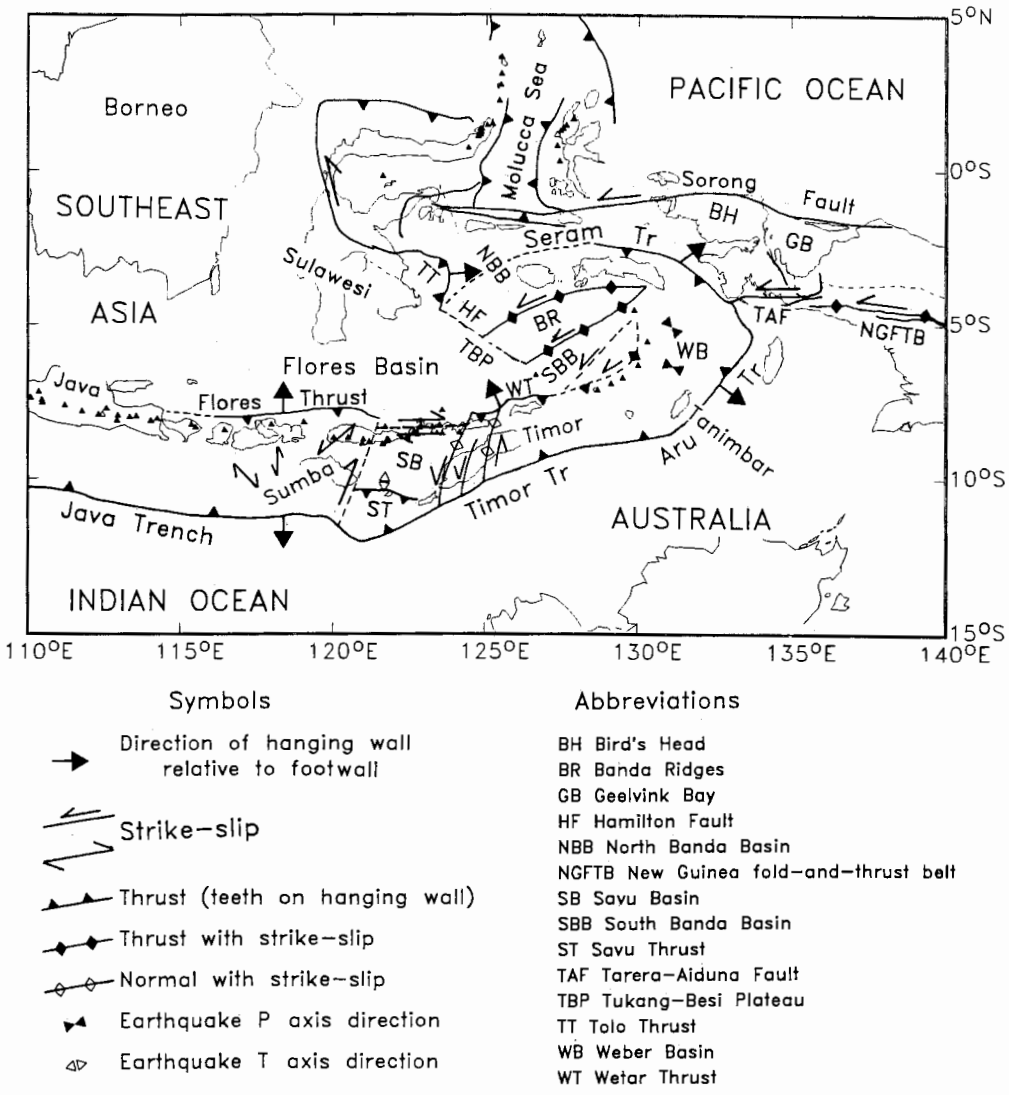

Fig. 8. Generalized tectonic map of the eastern Indonesia collision zone. The strike-slip faults on Timor are based on the work of T. Charlton and A. Barber (unpublished manuscript, 1987), and faults in the Sulawesi-Molucca Sea region are from Silver et al. [1983b] and Silver [1981].

and the forearc at Sumba, N-S, and does not change observably along its length. This observation and the westward decrease in the amount of strain along the Flores thrust [Silver et al., 1983a] indicate that the pole of rotation of the eastern Sunda forearc (from Bali to Sumba) with respect to SEA is located in eastern Java, probably near 114°E. This part of the Sunda forearc, which I will call the Sumba block, has gone through 2°-4° of counterclockwise rotation, depending on the total convergence taken up at the eastern end of the Flores thrust (estimated to be 30-60 km by Silver et al. [1983a]).

It is clear from the presence of large strike-slip earthquakes within the Sumba block that it does not rotate as a single rigid block, but instead it is disrupted internally. Slip vectors for thrust earthquakes on the Flores thrust zone and the strike-slip mechanisms beneath the forearc and arc constrain the type of deformation that produces the rotation of the forearc. One type that can be ruled out is a series of parallel NE trending, left-lateral strike-slip faults as these would produce NE trending slip vectors on the Flores thrust. A series of north trending left-lateral faults would produce the correct offset and slip vectors on the Flores thrust. This geometry is supported by the mechanism of event 52, but the remaining mechanisms (events 10, 40, and 54) show NW and NE trending nodal planes (Figure 3). The favored geometry is a set of left-lateral, NE trending and right-lateral, NW trending strike-slip faults. Slip evenly distributed between these two fault sets predicts the correct slip direction on the Flores thrust. This geometry is supported by evidence that the probable fault planes for events 10 and 54 are nearly orthogonal to that for event 40. Events 10 and 54 are aligned on a NE trend that is parallel to a series of lineations identified in side-looking airborne radar (SLAR) images of western Flores by Silver et al. [1983a], so these probably occurred

on NE trending, left-lateral faults. Aftershocks of event 40 were found to delineate a NW trend after relocation [Spence, 1986], suggesting that event 40 occurred on a NW trending, right-lateral fault.

The preferred geometry requires a shear zone to accommodate northward motion of the Sumba block with respect to the Savu Basin, shown in Figure 8 as a NNE trending right-lateral fault abutting the east coast of Sumba. The existence of this shear zone has not been documented but is suggested by the truncation of the Savu and Flores thrusts, again by structural lineations on central Flores [Silver et al., 1983a], by embayments in both the north and south coasts of Flores, and by changes in both the distribution of shallow earthquakes and the width of the active volcanic arc. The shear zone may end at the Savu thrust, although it does not appear to be active, or more likely continues south to the Java trench where its sense of offset is consistent with the jog in the trench axis.

The Savu Basin is shown as a separate block moving SSW with respect to both Sumba and Timor, west with respect to the Flores Basin, and SSW with respect to Australia (Figure 8). The northern boundary of the Savu block is inferred to be an east trending, right-lateral transform, suggested by the mechanism of event 56 (Figure 3), E-W structural lineations along the island arc north of the Savu Basin (e.g. the Solor Strait), and the near absence of back arc thrusting in this region. Limited thrusting does occur along along a NE trend at the west side of a NE trending promontory on easternmost Flores Island [Silver et al., 1983a]; such thrusting would result from the microplate geometry shown if the promontory moved with the Savu Basin block relative to the Flores Basin.

Southern Banda arc. The absence of large thrust earthquakes along the Timor trough raises questions about whether or not convergence between Australia and the Banda arc occurs there [Fitch, 1972]. Johnston and Bowin [1981] estimate that the convergence rate at the Timor trough near Timor is less than 10 mm/yr from variations in sedimentation rates at the site of Deep Sea Drilling Project (DSDP) hole 262. Karig et al. [1987] interpret marine seismic and swath-mapping profiles from a short section of the Timor trough south of western Timor and infer that the subduction rate is much higher, although they do not assign a value. They reasoned that shortening must occur by thrust faulting at the Timor trough, at the Wetar thrust, or in the Savu Basin, and so reached their conclusion by ruling out the latter two. This conclusion, however, ignores the possibilities raised by the earthquake mechanisms that the forearc is shortened by strike-slip faulting and that the Banda Basin accommodates some of the plate convergence. Moreover, Karig et al. [1987] examined the section of the Timor trough where subduction is predicted to be fastest, according to the geometry shown in Figure 8. The distribution of convergence across the collision zone both at the present time and since the collision of Australia with the arc began remains an outstanding question.

T. Charlton and A. Barber (unpublished manuscript, 1987) suggested that Timor is cut by a series of NNE to NE trending, left-lateral strike-slip and normal faults. They estimated that three such faults have accommodated a total of 100 km of left-lateral shear and that several lesser faults may account for more. In support of their suggestion, north of central Timor, the volcanic arc between Alor and Wetar (Figure 1) is offset along a NE trend by about 50 km in a left-lateral sense. The westernmost of their inferred faults, the Semau fault, may run from the Timor trough to the Wetar thrust and is thought here to be the present boundary between the Timor block and the Savu Basin block. Its northern end is inferred to intersect the western end of the Wetar thrust, and it separates the active from inactive segments of the volcanic arc. If so, then the displacement on the fault is roughly the same as that on the Wetar thrust, only a few kilometers. Event 30 (Figure 3) produced a complex pattern of ground fractures over a broad area with a NE trend in southwestern Timor and is interpreted by Tjia [1981] as due to NW directed compression and NE tension, roughly in accord with the fault plane solution determined here. Its duration (6 s) and the extent of the disrupted region [Tjia, 1981] suggests that it ruptured a distance of about 30 km. While the choice of the fault plane for this earthquake is not clear, its mechanism and sense of slip are consistent with a fault of the type proposed by Charlton and Barber.

The Timor block thrusts NW over the South Banda Basin (SBB) at the Wetar thrust and over Australia in the south. If the SBB and the Flores Basin form a rigid plate and there is no evidence to suggest otherwise, then the difference in the slip vectors at the Flores and Wetar thrusts suggest that the Timor and Sumba blocks converge. If Timor is moving toward Sumba, then convergence at the Timor trough is predicted to be NNE but this slip direction has yet to confirmed by direct observations.

The importance of the Wetar thrust zone as a modern site of crustal shortening is suggested by the concentration of $M \geq 7.0$ earthquakes during the past 90 years there [McCaffrey and Nabelek, 1986], two of which are known to be shallow and have thrust mechanisms (events 1 and 39). It is possible that faster slip occurs at the Timor trough than at the Wetar thrust, as suggested by Karig et al. [1987], but that the Wetar thrust is merely more seismic. In either case the Wetar thrust has not been important in the evolution of the collision zone as the total amount of convergence on it is small, probably less than 10 km [McCaffrey and Nabelek, 1986; Silver et al., 1983a].

NE striking left-lateral strike-slip faults and north striking normal faults within the forearc displace the eastern end of the forearc (Tanimbar) to the ENE relative to Timor and Sumba. As a result, Tanimbar moves NE with respect to Sumba, and because Sumba moves south with respect to Australia, Tanimbar has an eastward component of motion with respect to Australia. Such motion provides a mechanism for NW directed underthrusting at the Aru trough. From stratigraphic relations, Schlüter and Fritsch [1985] estimated that the convergence rate at the Aru trough SE of Tanimbar is 5 mm/yr, roughly in accord with the E-W extension rates for the forearc and back arc basin found here (2.9 and 1.2 mm/yr, respectively).

Earthquake mechanisms are consistent with a NW convergence direction at the Aru trough. First, P axes for strike-slip earthquakes beneath the Weber Basin trend NW, perpendicular to the trench.

Second, eastward migration of Tanimbar relative to Timor predicts that the slip vectors for thrust earthquakes between the arc and the SBB should rotate clockwise from west to east along the arc. Appropriately, assuming that the south dipping planes are the fault planes, the slip vector for event 32 at the eastern end of the Wetar thrust trends 184° (the strike of event 1 is poorly constrained; Table 1), while those for events 33 and 39 in the west trend 143° and 152°, respectively (Figure 3).

In a section across the convergent margin near eastern Timor, the full amount of convergence between the Australian continent and eastern Indonesia can be explained by a combination of shortening within the Banda Basin and at the Wetar thrust and thrusting of Australia beneath the forearc. Geologic evidence suggests that the leading edge of the Australian continental crust entered the Timor trough around 3 Ma [Abbott and Chamalaun, 1981; Carter et al., 1976; Hamilton, 1979; Karig et al., 1987] so that, for a convergence rate of 70 mm/yr, approximately 210 km of convergence has occurred since. Shortening across the Banda Basin and at the Wetar thrust acts to deflect the Timor trough and the island arc northward so an estimate of this shortening is the 50 km of northward displacement of Wetar with respect to Alor. The minimum amount that Australia has thrust beneath the forearc (150 km) is simply the distance between the present Timor trough and the northern limit of Australian crust, probably now beneath the north coast of Timor [Chamalaun et al., 1976; Hamilton, 1979]. Thus the amount of convergence explainable by shortening in the Banda Basin and by thrusting of Australia beneath the forearc is enough to account for the northward motion of the Australian continental crust since the collision began. The point is that subduction of continental crust into the mantle is not required by these geometrical considerations, although the foregoing analysis certainly does not prove that it has not occurred.

Banda Basin. I interpret that the strike-slip faulting beneath the Banda Basin accommodates NE motion of the South Banda Basin (SBB) relative to both the Banda Ridges (BR) and the North Banda Basin (NBB); this interpretation presumes that the NE trending nodal planes are the fault planes for the strike-slip earthquakes. Such faulting, along with thrust faulting at the Wetar thrust and within the Banda Basin, results in northward and eastward displacement of the Banda arc and forearc relative to the Sunda arc and Sulawesi (Figure 8). These displacements result in counterclockwise bending of the arc.

The wide distribution of thrust mechanisms at shallow depths indicates that back arc spreading does not occur at present in the Banda Basin, as proposed by Hamilton [1979]. To the contrary, the earthquakes show that the Banda Basin is closing. Easterly expansion of the Banda arc, which is the only evidence for Hamilton's spreading hypothesis, can be explained as well by strike-slip faulting, but in this case the expansion occurs without an increase in surface area of the back arc basin.

The geology of the BR and many of the islands around the Banda Basin suggests that much of the Banda Basin formed by accretion of crustal slivers detached from New Guinea [Silver et al., 1985], and the present crustal movements inferred from earthquake mechanisms provide a view of this process. Shallow earthquakes indicate that the BR and Seram are moving south and probably west with respect to the SBB. Prior to the initiation of subduction at the Seram trough, the movement of crustal blocks into the Banda Basin would have acted to increase its area. Slivers now represented by Buton [Katili, 1974], the Tukang-Besi Plateau, BR, and perhaps Buru and the SBB, arrived from the east and collided with the subduction zone in Sulawesi. Concurrently, the Java trench extended eastward as the Indian Ocean plate subducted beneath the accreted continental slivers and the SBB. The Bird's Head began to move westward with respect to Australia, and subduction started north of these slivers at the Seram trough, resulting in collision of the Bird's Head with Seram in the late Miocene [Audley-Charles et al., 1979] and 74° of counterclockwise rotation of Seram [Haile, 1981]. In the early Pliocene, Australia arrived at the Timor trough, and the continued eastward migration of the Banda arc resulted in the forearc overriding the continent at the Aru trough.

The Banda arc collision zone is clearly a setting for the accretion of terranes to a continental margin and as such offers some general insight into the process of terrane accretion. The major feature that stands out is the role of strike-slip faulting. Here we see a mechanism that differs greatly from a "conveyor belt" in which pieces of thick crust riding on subducting oceanic lithosphere are scraped off and plastered against the margin. The Banda Ridges have moved several hundred kilometers relative to their probable source region in northern New Guinea, motion which most likely occurred along transform faults as there are no indications that large oceanic basins have closed along their northern or southern margins where they now abut oceanic basins. At the present stage, however, earthquakes indicate that the ridges are bounded by faults with large thrust components and it appears that the small oceanic basins (Flores and South Banda basins) within the upper plate are starting to close.

In Alaska, some terranes are far-traveled and are often bounded by thrust faults yet the identification of the subduction zones that presumably accommodated thousands of kilometers of displacement can not be made [e.g., Jones et al., 1982]. The Banda Basin example suggests that the presence of a subduction zone, at least in the immediate vicinity of the accreted blocks, is not necessary. If the Banda Ridges are indeed part of northern New Guinea, then they moved north with the Australian plate several thousand kilometers relative to their present position [e.g., Dietz and Holden, 1970], but the subduction zone that accommodated this motion is probably buried in New Guinea [Hamilton, 1979] and not in the Banda Basin. The present tectonics of the Banda Basin also demonstrates that in the final stages of collision the strike-slip faults along which these slivers originally moved into place can become thrusts, where small oceanic basins are closed, and the original emplacement geometry can be obscured quickly.

Relationship of the Timor, Aru, and Seram troughs. At its eastern end the Timor trough bends to a more northeasterly trend into the Aru trough and then westward into the Seram trough

(Figure 1). Structural continuity in the arc structure is suggested by many geological and geophysical features to at least 4°S where there are breaks in the active volcanic arc, seismicity, bathymetry, and gravity, but the outer arc ridge appears to be continuous [Bowin et al., 1980; Hamilton, 1979]. Bathymetry and seismic profiles suggest that continental crust forms the floor of the trenches all the way around the bend from Timor to Seram [Jacobson et al., 1979; von der Borch, 1979], but it is not clear whether or not the same plate is being subducted at the Timor, Aru, and Seram troughs, as has been suggested, primarily by Hamilton [1979], but disputed by others [Bowin et al., 1980; Cardwell and Isacks, 1978; McCaffrey, 1988].

The present style of deformation within the Banda Basin, inferred from shallow earthquake mechanisms, requires convergence between the Bird's Head, which subducts at the Seram trough, and Australia, which subducts beneath the Timor and Aru troughs, and so favors the two-plate view. Slip vectors of underthrust earthquakes show that Sumba moves at an azimuth of 177°±5° with respect to Australia and that Seram moves at 52°±15° with respect to the Bird's Head (BH) of western New Guinea. Independent of assumed rates, in order to have subduction at the Seram trough with the condition that BH is part of Australia, Seram has to move NNE with respect to Sumba at a rate faster than Australia moves north with respect to Sumba. This scenario predicts NNE extension between Sumba and Seram. Earthquakes beneath the Banda Basin, however, invariably show shortening between Sumba and Seram and evidence for extension is lacking, so the single-plate hypothesis is unlikely.

Since earthquakes in the Banda Basin show that Sumba and Seram converge, it follows that Bird's Head is moving SSW to SW with respect to Australia; the actual direction depends on the various relative rates, which are unknown. This requires motion between Australia and the BH along faults in western Irian Jaya. Likely sites for such motion are the New Guinea fold-and-thrust belt and the Tarera-Aiduna fault zone as suggested by Cardwell and Isacks [1978]. The history of the Tarera-Aiduna fault is unknown, but large, left-lateral strike-slip earthquakes occur east of its mapped trace suggesting that it extends into the Highlands of New Guinea [Abers and McCaffrey, 1988]. Alternatively, the eastern margin of Geelvink Bay has been cited as a possible site for slip [Dow and Sukamto, 1984]. In either case the Aru Basin marks the northern edge of the Aru trough and the Seram trough is separate, subducting the Bird's Head which is not part of the Australian plate. The Aru Basin contains a trench-trench-transform triple junction, which is a stable configuration since both trenches accommodate subduction beneath the same plate.

Conclusions

The mechanism of collision of the Australian continent with the East Sunda and Banda island arcs is examined. Depths and fault plane solutions of large earthquakes are estimated from their long-period, teleseismic P and SH waves and are used to constrain the active, shallow tectonics of the collision zone. The purpose of using body waves is that they allow the estimation of centroidal depths with an uncertainty of 5 km or less. Such constraints have allowed distinction between upper and lower plate earthquakes, and a much clearer picture of how deformation occurs in the collision zone has emerged.

The convergence of the Australian continent with eastern Indonesia is accommodated to some degree by N-S crustal shortening throughout the forearc, arc, and back arc regions. Beneath the forearc but within the upper plate, strike-slip and normal faulting prevails and the earthquakes' T axes are aligned parallel to the arc. The forearc apparently expands in the E-W direction, normal to the convergence direction as it contracts in the N-S direction. Earthquake mechanisms suggest that the forearc does not now deform by internal thrusting (and crustal thickening) but instead that it is being pushed northward over the back arc basin and squeezed out to the side by the encroaching Australian continent. Lateral movement of the forearc by strike-slip faulting might occur only because the bend in the eastern end of the Timor trough leaves the forearc unbound in that direction.

Within the back arc (the Banda Basin), strike-slip and thrust faulting reveal convergence between Timor and Seram. Strike-slip faulting within the Banda Basin also produces eastward migration of the eastern Banda arc and can explain the younger volcanics and shorter subducted slab in the east than in the west without calling on back arc spreading in the Banda Basin. The surface area of the Banda Basin is being decreased by thrust faulting.

The Bird's Head of Irian Jaya is not now part of the Australian plate. Slip vectors for earthquakes at the Seram trough show WSW underthrusting of the Bird's Head beneath Seram and, coupled with N-S shortening in the Banda Basin, indicate that the Bird's Head moves to the WSW with respect to Australia. The preferred decoupling zone between the Bird's Head and Australia is in the New Guinea fold-thrust belt and the Tarera-Aiduna fault zone in western New Guinea.

Back arc thrusting plays an important role in the convergence across the collision zone, but earthquakes do not substantiate a reversal in the direction of subduction. Slip vectors for the back arc thrust earthquakes roughly parallel the direction of relative motion between the Indian Ocean-Australia plate and Indonesia, suggesting that collision with Australia or coupling of the upper plate with the Indian Ocean plate in general is driving the back arc thrusting. A back arc thrust zone south of Ambon has been identified by shallow earthquakes.

Earthquakes suggest that the lithosphere of the Weber Basin sits directly on the subducting plate, without intervening asthenosphere, so that the basin formed as a result of sinking of the subducting plate.

The Banda Basin probably formed as slices of northern New Guinea were transported westward with the Pacific plate and collided with an island arc in eastern Sulawesi. Earthquakes within the Banda Basin show that this process is probably continuing today as the Banda Ridges and Seram slide west and south with respect to the Banda arc by strike-slip and thrust faulting. Eventually, these former pieces of northern New Guinea will be emplaced on the Australian margin by thrusting after a long history of translation along it.

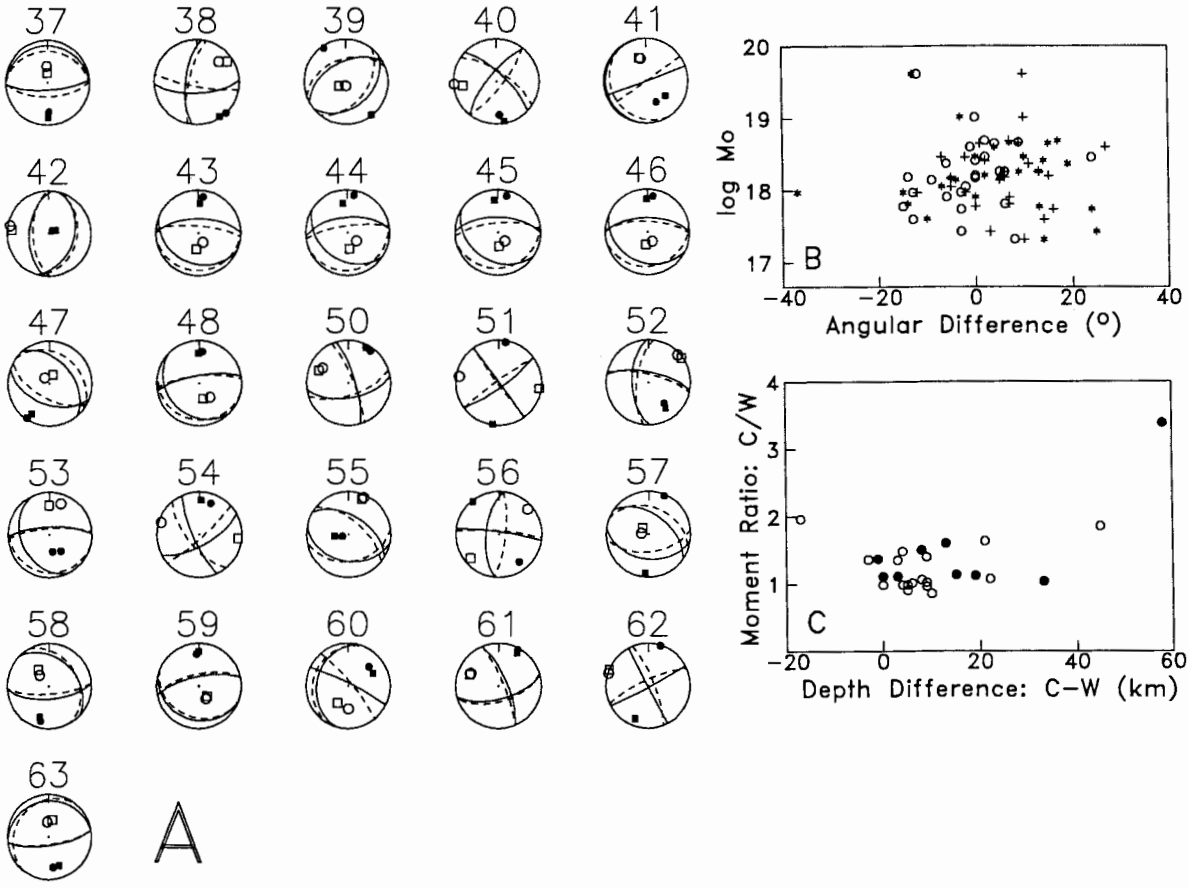

Fig. 9. (a) Comparison of fault plane solutions (P wave nodal planes) determined by body waveform modeling (solid lines) to the best fitting double couples from the Harvard centroid moment tensor solutions (dashed lines). Solid and open symbols show the P and T axes; circles for the waveform solutions and squares for the CMT solutions. (b) Plot of differences in strike (circles), dip (crosses), and rake (asterisks) against seismic moment. (c) Plot of differences in the depths of CMT and waveform solutions versus their moment ratios. (C, CMT solution; W, waveform solution.) In Figure 9c the solid circles represent strike-slip events, while open circles show dip-slip events.

Appendix 1

Comparison of Waveform Solutions to Centroid Moment Tensor Solutions

Twenty-six earthquakes in this study have centroid moment tensor (CMT) solutions determined [e.g., Dziewonski et al., 1981]. Because we use shorter-period data and a different approach to extract much of the same information, it is useful to compare results. Disagreement would diagnose a problem in one or both approaches, while agreement gives confidence in both. In general, the orientations of the double couples are encouragingly similar; the differences are -1°±8° in strike ϕ, 5°±9° in dip δ, and 5°±11° in rake λ (Figures 9a and 9b). The one outlier for rake is from event 56.

The very long period data used in the CMT solutions are much less sensitive to source depths in the upper 50 km than are the World-Wide Standardized Seismograph Network (WWSSN) seismograms [Dziewonski et al., 1981]. The CMT depths are systematically greater than the waveform depths; nine of the CMT solutions are more than 10 km deeper than those constrained by body waves, while only two determined in this study are deeper than the CMT (Figure 9c). Seismic moments for most events agree within a few percent, but for a couple the CMT moment is a factor of 2 greater than that determined from body waves. There seems to be little correlation of moment ratio with depth differences (Figure 9c).

Examples of Waveforms and Solutions

Four selected events (Figure 10) serve to characterize the solutions and the observed seismograms. Event 5 is an underthrusting earthquake from the Seram trough at a depth of 21 km. Amplitudes of the observed seismograms are matched well except for the P wave at station SBA, which is often a factor of 2 larger than predicted. The variation among the observed seismograms can be seen by comparing the P waves at neighboring stations, as they are predicted to have nearly identical waveforms. Seismograms from the Asian stations HOW, SHI, NDI, QUE, CHG, NHA, and SHL display great similarity indicating that receiver crustal and upper mantle structures are similar beneath these stations (the same mantle propagation corrections and receiver structures are

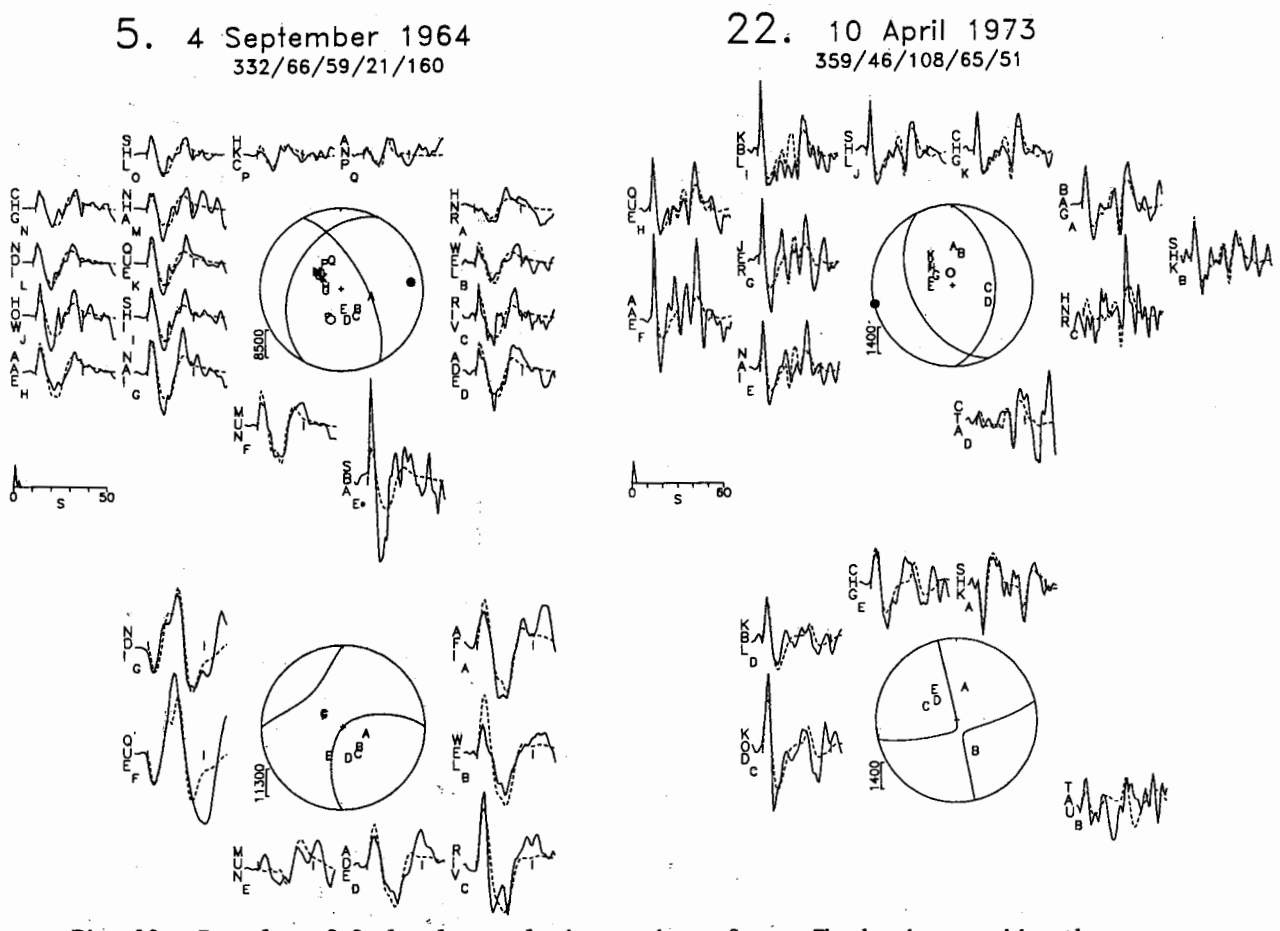

Fig. 10. Examples of fault plane solutions and waveforms. The header provides the event number and date followed by the solution parameters in the form strike/dip/rake/depth/M_o (depth is in kilometers and M_o is $\times 10^{16}$ N m). Observed seismograms are shown by solid lines, and synthetic seismograms are shown by dashed lines. Vertical bars enclose the data used in the inversion, and an asterisk indicates that the seismogram was not used. Seismogram amplitudes correspond to the same instrument magnification and same epicentral distance so that the variations among them are preserved. The station code is at the left of each seismogram, and the single letter identifies its position on the focal sphere. P waveforms are shown at the top and SH at the bottom of each plot. Solid and open circles in the P focal sphere show the P and T axes, respectively. The amplitude scale at the lower left of each focal sphere is labeled in microns; this scale corresponds to an instrument of magnification 3000 at an epicentral distance of 40°. Note that the scale may be different for P and SH waves. The normalized source time function is shown on the time axis. For the double event (number 52), the P and SH nodal surfaces and the source time function for the second event are shown by dashed lines. All solutions are shown in this format in Appendix 3 on microfiche.

assumed for all stations in generating the synthetics). Stations WEL, RIV, and ADE to the southeast, however, show more variation in both the P and SH waves, probably because of greater differences in structure along the ray path to and beneath these stations.

Event 22 occurred beneath Sumba Island and its depth, 65 km, is indicated by clear reflected phases late in the waveform that interfere little with the direct arrival. The first pulse is simple and constrains the source duration to within ±1 s. Waveforms for this event show the variation in the part of the seismograms comprising reflected phases. While the seismograms to the west and north show strong coherence, those to the southeast (HNR and CTA) are quite different from each other, particularly in frequency.

Event 51 is a shallow strike-slip event from the south Banda Basin whose source is short enough so that the reflected phases in the P waves are separated in time from the direct arrival (for example, in the P wave at HNR). The nodal planes are constrained well because the seismograms are very sensitive to their orientations, but often poor fits to the observed seismograms result from this sensitivity. Notice also that the SH waves are much larger in amplitude than the P waves, which is diagnostic of strike-slip mechanisms, whereas in the previous dip-slip mechanisms P and SH waves were of similar sizes (note amplitude scales beside focal spheres in Figure 10).

Finally, event 52, from south of eastern Sumbawa, was the only earthquake modeled with multiple sources of different orientations. A mul-

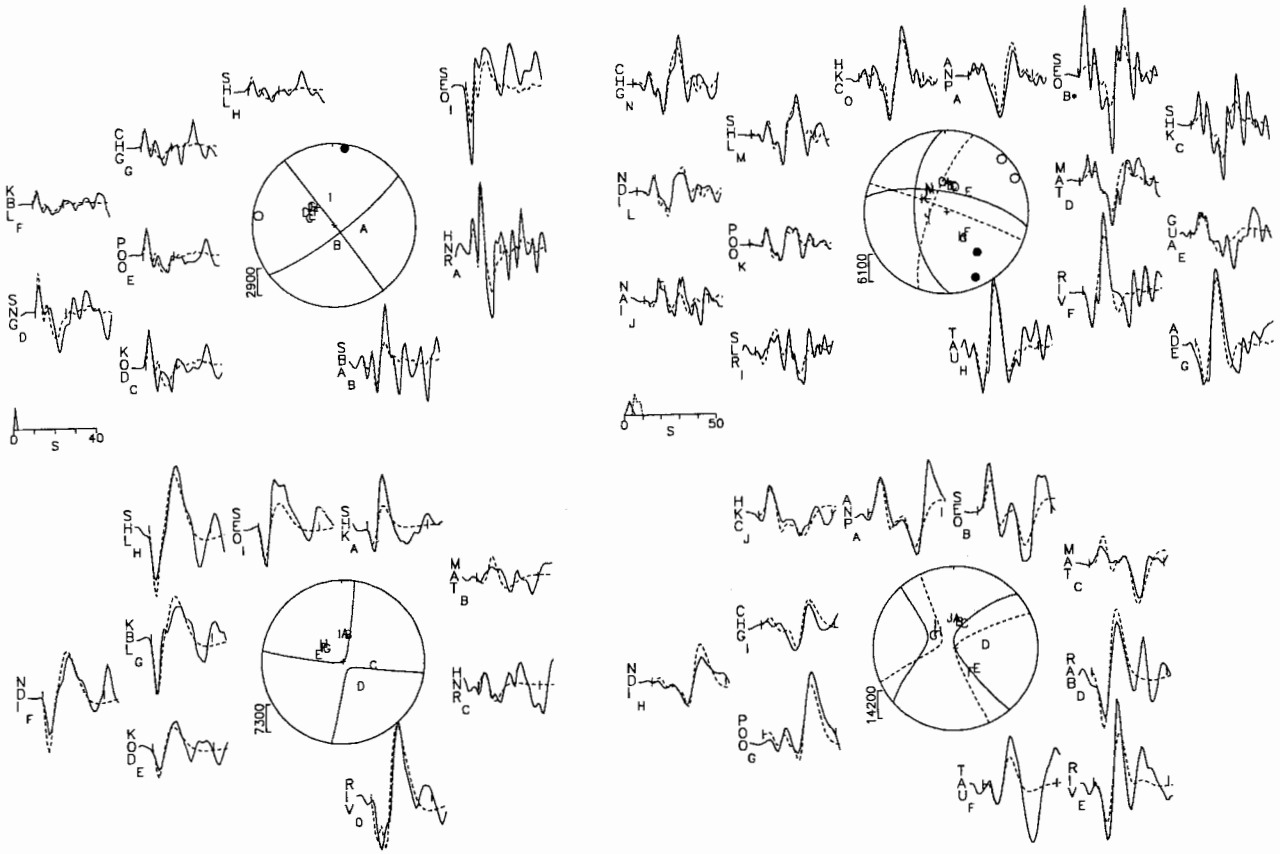

Fig. 10. (continued)

tiple source was evident because the initial pulses on P wave seismograms to the west and NW (e.g., SLR, NAI, POO, NDI, SHL, and CHG) were inconsistent with the single-source solution that fit the seismograms best. The first subevent (whose nodal surfaces are shown by solid lines) contains a slightly greater component of normal faulting than the second subevent (dashed lines) that commenced 4 s later. The second event was larger, accounting for 64% of the total moment, and possibly occurred at a slightly greater depth. Again this example points out the sensitivity of the waveforms to small changes in the orientation of strike-slip events; a similar change in orientation of a dip-slip event would not be evident.

Acknowledgments. This work benefited greatly from discussions with Geoff Abers and John Nabelek about waveforms and Indonesia. Dan Karig provided a thorough review and Justin Revenaugh and Anne Sheehan helped with computing. Work on the Sunda arc earthquakes was started under NSF grant EAR-8319250 and was extended to the Banda arc with support of the Air Force Geophysics Scholars Program, sponsored by the Air Force Geophysics Laboratory, United States Air Force, under contract F19628-86-C-0224 to the Southeast Center for Electrical Engineering Education.

References

Abbott, M., and F. Chamalaun, Geochronology of some Banda arc volcanics, in The Geology and Tectonics of Eastern Indonesia, Spec. Publ. 2, edited by A. Barber and S. Wiryosujono, pp. 253-268, Geological Research and Development Centre, Bandung, Indonesia, 1981.

Abers, G., and R. McCaffrey, Active deformation in the New Guinea fold-and-thrust belt: Seismological evidence for strike-slip faulting and basement-involved thrusting, J. Geophys. Res., in press, 1988.

Aki, K., and P. Richards, Quantitative Seismology, Theory and Methods, 557 pp., W. H. Freeman, New York, 1980.

Audley-Charles, M., and J. Milsom, Comment on 'Plate convergence, transcurrent faults, and internal deformation adjacent to southeast Asia and the western Pacific,' J. Geophys. Res., 79, 4980-4981, 1974.

Audley-Charles, M., D. Carter, A. Barber, M. Norvick, and S. Tjokrosapeotro, Reinterpretation of the geology of Seram: Implications for the Banda arcs and northern Australia, J. Geol. Soc. London, 136, 547-568, 1979.

Bowin, C., G. Purdy, C. Johnston, G. Shor, L. Lawver, H. M. S. Hartono and P. Jezek, Arc-continent collision in the Banda Sea region, Am. Assoc. Pet. Geol. Bull., 64, 868-915, 1980.

Brune, J., Seismic moment, seismicity, and rate of slip along major fault zones, J. Geophys. Res., 73, 777-784, 1968.

Cardwell, R., and B. Isacks, Geometry of the subducted lithosphere beneath the Banda Sea in eastern Indonesia from seismicity and fault plane solutions, J. Geophys. Res., 83, 2825-2838, 1978.

Cardwell, R., E. Kappel, M. Lawrence, and B. Isacks, Plate convergence along the Indonesian arc (abstract), Eos Trans. AGU, 62, 404, 1981.

Carter, D., M. Audley-Charles, and A. Barber, Stratigraphical analysis of island arc-continental margin collision in eastern Indonesia, J. Geol. Soc. London, 132, 179-198, 1976.

Chamalaun, F., K. Lockwood, and A. White, The Bouguer gravity field of eastern Timor, Tectonophysics, 30, 241-259, 1976.

Cooper, P., and B. Taylor, Seismotectonics of New Guinea: A model for arc reversal following arc-continent collision, Tectonics, 6, 53-67, 1987.

Dalmayrac, B., and P. Molnar, Parallel thrust and normal faulting in Peru and constraints on the state of stress, Earth Planet. Sci. Lett., 55, 473-481, 1981.

Dewey, J., and J. Bird, Mountain belts and the new global tectonics, J. Geophys. Res., 75, 2625-2647, 1970.

Dietz, R., and J. Holden, Reconstruction of Pangaea: Breakup and dispersion of continents, Permian to present, J. Geophys. Res., 75, 4939-4956, 1970.

Dow, D., and R. Sukamto, Western Irian Jaya: The end product of oblique plate convergence in the late Tertiary, Tectonophysics, 106, 109-139, 1984.

Duda, S., Secular seismic energy release in the circum-Pacific belt, Tectonophysics, 2, 409-452, 1965.

Dziewonski, A., T.-A. Chou, and J. Woodhouse, Determination of earthquake source parameters from waveform data for studies of global and regional seismicity, J. Geophys. Res., 86, 2825-2852, 1981.

Fitch, T., Plate convergence, transcurrent faults, and internal deformation adjacent to southeast Asia and the western Pacific, J. Geophys. Res., 77, 4432-4460, 1972.

Fitch, T., and P. Molnar, Focal mechanisms along inclined earthquake zones in the Indonesian-Philippine region, J. Geophys. Res., 75, 1431-1444, 1970.

Fitch, T., R. North, and M. Shields, Focal depths and moment tensor representations of shallow earthquakes associated with the great Sumba earthquake, J. Geophys. Res., 86, 9357-9374, 1981.

Gutenberg, B., and C. Richter, Seismicity of the earth and related phenomena, 310 pp., Princeton University Press, Princeton, N. J., 1954.

Haile, N., Palaeomagnetic evidence and the geotectonic history and palaeogeography of eastern Indonesia, in The Geology and Tectonics of Eastern Indonesia, Spec. Publ. 2, edited by A. Barber and S. Wiryosujono, pp. 81-87, Geological Research and Development Centre, Bandung, Indonesia, 1981.

Hamilton, W., Earthquake map of the Indonesian region, U.S. Geol. Surv. Misc. Invest. Ser. Map, I-875-C, 1974.

Hamilton, W., Subduction in the Indonesian region, in Island Arcs, Deep Sea Trenches, and Back-Arc Basins, Maurice Ewing Ser., vol. 1, edited by M. Talwani and W. Pitman III, pp. 15-31, AGU, Washington, D. C., 1977.

Hamilton, W., Tectonics of the Indonesian region, U.S. Geol. Surv. Prof. Pap., 1078, 345 pp., 1979.

Helmberger, D., Generalized ray theory for shear dislocation, Bull. Seismol. Soc. Am., 64, 45-64, 1974.

Jacobson, R., G. Shor, R. Kieckhefer, and G. Purdy, Seismic refraction and reflection studies in the Timor-Aru trough system and Australian continental shelf, Mem. Am. Assoc. Pet. Geol., 29, 209-222, 1979.

Johnson, R., and A. Jaques, Continent-arc collision and reversal of arc polarity: new interpretations from a critical area, Tectonophysics, 63, 111-124, 1980.

Johnston, C., and C. Bowin, Crustal reactions resulting from the mid Pliocene to Recent continent-island arc collision in the Timor region, BMR J. Aust. Geol. Geophys., 6, 223-243, 1981.

Jones, D., N. Silberling, W. Gilbert, and P. Coney, Character, distribution, and tectonic significance of accretionary terranes in the Central Alaska Range, J. Geophys. Res., 87, 3709-3717, 1982.

Kappel, E., Plate convergence in the Sunda and Banda arcs, B.A. thesis, 40 pp., Cornell Univ., Ithaca, N. Y., 1980.

Karig, D., A. Barber, T. Charlton, S. Klemperer, and D. Hussong, Nature and distribution of deformation across the Banda arc-Australian collision zone at Timor, Geol. Soc. Am. Bull., 98, 18-32, 1987.

Katili, J., Geological environment of the Indonesian mineral deposits, Geol. Surv. Indones. Econ. Geol. Ser., 7, 1-18, 1974.

Kelleher, J., and W. McCann, Buoyant zones, great earthquakes, and unstable boundaries of subduction, J. Geophys. Res., 81, 4885-4896, 1976.

Kostrov, B., Seismic moment and energy of earthquakes, and seismic flow of rocks, Izv. Acad. Sci. USSR Phys. Solid Earth, Engl. Transl., 1, 23-44, 1974.

Langston, C., and D. Helmberger, A procedure for modeling shallow dislocation sources, Geophys. J. R. Astron. Soc., 42, 117-130, 1975.

Larson, R., Late Jurassic sea-floor spreading in the eastern Indian Ocean, Geology, 3, 69-71, 1975.

Lockridge, P., and R. Smith, Tsunamis in the Pacific Basin 1900-1983, Nat. Geophys. Data Cent., Boulder, Co., 1984.

Mammerickx, J., R. Fisher, F. Emmel, and S. Smith, Bathymetry of the east and southeast Asian seas, Geol. Soc. Am. Map Chart Ser., MC-17, 1976.

McCaffrey, R., Seismological constraints and speculations on Banda Arc tectonics, Netherlands J. Sea Res., in press, 1988.

McCaffrey, R., and G. Abers, SYN3: A microcomputer program for inversion of teleseismic body waveforms, AFGL Tech. Rep. AFGL-TR-88-0099, Air Force Geophys. Lab., Bedford, Mass., 1988.

McCaffrey, R., and J. Nabelek, The geometry of back arc thrusting along the eastern Sunda arc, Indonesia: Constraints from earthquake and gravity data, J. Geophys. Res., 89, 6171-6179, 1984.

McCaffrey, R., and J. Nabelek, Seismological evidence for shallow thrusting north of the Timor trough, Geophys. J. R. Astron. Soc., 85, 365-381, 1986.

McCaffrey, R., and J. Nabelek, Earthquakes, gravity and origin of the Bali Basin: An example of a nascent continental fold-and-thrust belt, J. Geophys. Res., 92, 441-460, 1987.

McCaffrey, R., P. Molnar, S. Roecker and Y. Joyodiwiryo, Microearthquake seismicity and fault plane solutions related to arc-continent collision in the eastern Sunda arc, Indonesia, J. Geophys. Res., 90, 4511-4528, 1985.

McKenzie, D., Speculations on the consequences and causes of plate motion, Geophys. J. R. Astron. Soc., 18, 1-18, 1969.

Minster, J., and T. Jordan, Present-day plate motions, J. Geophys. Res., 83, 5331-5354, 1978.

Molnar, P., Average regional strain due to slip on numerous faults of different orientations, J. Geophys. Res., 88, 6430-6432, 1983.

Molnar, P., and D. Gray, Subduction of continental lithosphere: Some constraints and uncertainties, Geology, 7, 58-62, 1979.

Molnar, P., and P. Tapponnier, Cenozoic tectonics of Asia: Effects of a continental collision, Science, 189, 419-426, 1975.

Molnar, P., D. Freedman and J. Shih, Lengths of intermediate and deep seismic zones and temperatures in downgoing slabs of lithosphere, Geophys. J. R. Astron. Soc., 56, 41-54, 1979.

Nabelek, J., Determination of earthquake source parameters from inversion of body waves, Ph.D. thesis, Mass. Inst. of Technol., Cambridge, 1984.

Nabelek, J., Geometry and mechanism of faulting of the 1980 El Asnam, Algeria, earthquake from inversion of teleseismic body waves and comparison with field observations, J. Geophys. Res., 90, 12,713-12,728, 1985.

Nelson, M., R. McCaffrey, and P. Molnar, Source parameters for 11 earthquakes in the Tien Shan, Central Asia, determined by P and SH waveform inversion, J. Geophys. Res., 92, 12,629-12,648, 1987.

Newcomb, K., and W. McCann, Seismic history and seismotectonics of the Sunda arc, J. Geophys. Res., 92, 421-439, 1987.

Osada, M., and K. Abe, Mechanism and tectonic implications of the great Banda Sea earthquake of November 4, 1963, Phys. Earth Planet. Inter., 25, 129-139, 1981.

Schlüter, H., and J. Fritsch, Geology and tectonics of the Banda arc between Tanimbar Island and Aru Island (Indonesia), Geol. Jahrb., Reihe E, 30, 41 pp., 1985.

Silver, E., A new tectonic map of the Molucca Sea and east Sulawesi, Indonesia, with implications for hydrocarbon potential and metallogenesis, in The Geology and Tectonics of Eastern Indonesia, Spec. Publ. 2, edited by A. Barber and S. Wiryosujono, pp. 343-347, Geological Research and Development Centre, Bandung, Indonesia, 1981.

Silver, E., D. Reed, R. McCaffrey, and Y. Joyodiwiryo, Backarc thrusting in the eastern Sunda arc, Indonesia: A consequence of arc-continent collision, J. Geophys. Res., 88, 7429-7448, 1983a.

Silver, E., R. McCaffrey and R. Smith, Collision, rotation, and the initiation of subduction in the evolution of Sulawesi, Indonesia, J. Geophys. Res., 88, 9407-9418, 1983b.

Silver, E., J. Gill, D. Schwartz, H. Prasetyo, and R. Duncan, Evidence for a submerged and displaced continental borderland, north Banda Sea, Indonesia, Geology, 13, 687-691, 1985.

Silver, E., N. Breen, H. Prasetyo, and D. Hussong, Multibeam study of the Flores back arc thrust belt, Indonesia, J. Geophys. Res., 91, 3489-3500, 1986.

Simkin, T., L. Siebert, L. McClelland, D. Bridge, C. Newhall, and J. Latter, Volcanoes of the World, 232 pp., Hutchinson Ross, Stroudsburg, Pa., 1981.

Spence, W., The 1977 Sumba earthquake series: Evidence for slab pull force acting at a subduction zone, J. Geophys. Res., 91, 7225-7239, 1986.

Stagg, H., and N. Exon, Geology of the Scott Plateau and Rowley Rise, Bull. Bur. Miner. Resour., 213, 67 pp., 1981.

Stein, S., and D. Wiens, Depth determination for teleseismic earthquakes: Methods and results, Rev. Geophys., 24, 806-832, 1986.

Tjia, H., Examples of young tectonism in eastern Indonesia, in The Geology and Tectonics of Eastern Indonesia, Spec. Publ. 2, edited by A. Barber and S. Wiryosujono, pp. 89-104, Geological Research and Development Centre, Bandung, Indonesia, 1981.

Turcotte, D., and G. Schubert, Geodynamics, 450 pp., John Wiley, New York, 1982.

Usna, I., S. Tjokrosapoetro, and S. Wiryosujono, Geological interpretation of a seismic reflection profile across the Banda Sea between Wetar and Buru islands, Bull. Geol. Res. Dev. Cent. Indones., 1, 7-15, 1979.

von der Borch, C., Continent-island arc collision in the Banda arc, Tectonophysics, 54, 169, 1979.

Wiens, D., Effects of bathymetry on teleseismic P waveforms (abstract), Eos Trans. AGU, 67, 1105, 1986.

R. McCaffrey, Department of Geology, Rensselaer Polytechnic Institute, Troy, NY 12180.

(Received November 13, 1987;
revised May 22, 1988;
accepted July 24, 1988.)